FAKULTÄT FÜR !NFORMATIK
Faculty of Informatics

Non-negative Matrix Factorization as a Tool for fMRI Analysis of Dynamicity and Individuality of Functional Networks

DIPLOMARBEIT

zur Erlangung des akademischen Grades

Diplom-Ingenieur

im Rahmen des Studiums

eingereicht von

Christoph Fürböck, BSc
Matrikelnummer 01303486

an der Fakultät für Informatik

der Technischen Universität Wien

Betreuung: Ao. Univ. Prof. Dipl.-Ing. Dr.techn. Robert Sablatnig
Mitwirkung: Assoc. Prof. Dipl.-Ing. Dr. Georg Langs

Wien, 16. November 2020

Christoph Fürböck	Robert Sablatnig

Technische Universität Wien
A-1040 Wien ▪ Karlsplatz 13 ▪ Tel. +43-1-58801-0 ▪ www.tuwien.ac.at

FAKULTÄT FÜR !NFORMATIK
Faculty of Informatics

Non-negative Matrix Factorization as a Tool for fMRI Analysis of Dynamicity and Individuality of Functional Networks

DIPLOMA THESIS

submitted in partial fulfillment of the requirements for the degree of

Diplom-Ingenieur

in

Biomedical Engineering

by

Christoph Fürböck, BSc
Registration Number 01303486

to the Faculty of Informatics

at the TU Wien

Advisor: Ao. Univ. Prof. Dipl.-Ing. Dr.techn. Robert Sablatnig
Assistance: Assoc. Prof. Dipl.-Ing. Dr. Georg Langs

Vienna, 16th November, 2020

Christoph Fürböck | Robert Sablatnig

Technische Universität Wien
A-1040 Wien ▪ Karlsplatz 13 ▪ Tel. +43-1-58801-0 ▪ www.tuwien.ac.at

Erklärung zur Verfassung der Arbeit

Christoph Fürböck, BSc

Hiermit erkläre ich, dass ich diese Arbeit selbständig verfasst habe, dass ich die verwendeten Quellen und Hilfsmittel vollständig angegeben habe und dass ich die Stellen der Arbeit – einschließlich Tabellen, Karten und Abbildungen –, die anderen Werken oder dem Internet im Wortlaut oder dem Sinn nach entnommen sind, auf jeden Fall unter Angabe der Quelle als Entlehnung kenntlich gemacht habe.

Wien, 16. November 2020

Christoph Fürböck

Danksagung

An dieser Stelle möchte ich mich bei allen bedanken, die mich beim Erarbeiten und Verfassen dieser Diplomarbeit unterstützt haben. Allen voran bei meinen Eltern und meiner Familie, denn nur durch deren durchgehende Unterstützung, welche weit über das Maß der Selbstverständlichkeit hinaus geht, war es für mich überhaupt möglich bis hierher zu kommen. Ganz besonders bedanke ich mich zudem bei Prof. Georg Langs für die kontinuierliche Hilfe und Beratung. Die Formulierung dieser Arbeit wäre ohne dem gemeinsamen Besprechen der Ergebnisse und der Weiterentwicklung von Konzepten und Ideen unvorstellbar gewesen. Danke für die Begleitung vom Beginn einer Projektarbeit bis zum Abschluss dieser Diplomarbeit!

Zusätzlich möchte ich mich bei allen Kollegen vom CIR für die freundliche Zusammenarbeit bedanken. Insbesondere gilt dieser Dank Karl Heinz, der immer ein offenes Ohr für spezifische Fragen hatte und mir nicht nur einmal weiterhelfen konnte.

Außerdem bedanke ich micht bei Aristeidis Sotiras, dessen Code meine Arbeit auf ein höheres Niveau heben konnte. Zudem war er eine große Hilfe bei der Implementierung und Verwendung davon.

Nicht zuletzt möchte ich mich herzlich bei Prof. Robert Sablatnig bedanken, der mir damals nahegelegt hatte, diesen Weg zu beschreiten und in den folgenden Jahren ein stetiger Begleiter für mich war.

Acknowledgements

At this point I would like to thank everyone who supported me in the process of writing this thesis. First of all I would like to thank my parents and family for the constant support that far exceeds any casual norm, which enabled me to get to this point. I cannot express my appreciation for the continuous help and advice of Prof. Georg Langs. The formulation of this thesis would have been impossible without the mutual discussion of the results and the progressive development and enhancement of concepts and ideas. Thank you for the continued supervision from the beginning of a project to the final thesis!

In addition I really appreciated the friendly cooperation with everyone of the CIR lab. Especially Karl Heinz has my gratitude for listening to my specific questions and helping me out more than once.

Moreover I am really grateful for the collaboration with Aristeidis Sotiras who helped me in the provision of the code as well as the support in the implementation and use of it.

Last but not least I sincerely thank Prof. Robert Sablatnig who had suggested this path to me in the first place and has been on my side since.

Kurzfassung

Funktionelle Magnetresonanztomographie (fMRT oder fMRI) liefert detaillierte Information über die Gehirnaktivität, die in dieser Arbeit mit Nicht-negativer Matrixfaktorisierung (NMF) analysiert wird. Das Ergebnis ist eine Einteilung des Gehirns in Regionen, welche reproduzierbar und interpretierbar ist. Diese Regionen spiegeln Einheiten wider, die sich funktional ähnlich verhalten. NMF erzeugt für jede Testperson individualisierte Ergebnisse, welche innerhalb derselben Person (*within*) und gegenüber den anderen Personen (*across*) verglichen werden. Der Vergleich zeigt eine hohe *within* Reproduzierbarkeit (Korrelation = 0.89) und hohe *across* Variabilität (Korrelation = 0.74) mit einem signifikanten Unterschied ($p < 0.001$). In diesem Kontext werden Werte für die Individualität und Dynamizität berechnet und zu bekannten Regionen in Bezug gesetzt um den Vergleich zur State-of-the-Art Forschung zu ermöglichen. Die individualisierten Ergebnisse werden verwendet um ein Vorhersagemodell zu erstellen, das die Hirnaktivierung während verschiedenen Aufgaben ausschließlich mit Daten im Ruhezustand verhersagen kann. Die Qualität der Vorhersage ist abhängig von der jeweiligen Aufgabe (Korrelation zwischen tatsächlicher und vorhergesagter Aktivierung 0.3 - 0.6) wobei die Signifikanz für alle Aufgaben außer einer hoch ist ($p < 0.001$). Die Koeffizienten der Individualität und Dynamizität werden verwendet um ein lineares Modell zu trainieren welches exemplarisch fluide Intelligenz vorhersagt. Die besten Ergebnisse liefert hier der Koeffizient der Individualität (Correlation zwischen tatsächlichem und vorhergesagtem Wert 0.32).

Abstract

Functional magnet resonance imaging (fMRI) scans provide detailed information of brain activities and are analysed in this work using Non-negative Matrix Factorization (NMF) resulting in a parcellation of the brain that is highly reproducible and interpretable. These regions represent areas that display functional similarity. NMF creates individual-specific results that are compared within the same subject and across different subjects. The individualized results demonstrate high within-subject reproducibility (correlation = 0.89) and high across-subject variability (correlation = 0.74) as well as a significant difference ($p < 0.001$). In this context values for individuality and dynamicity are calculated and the relation to known regions is established to enable a comparison to state of the art research. The individualized results are used to create a prediction model capable of predicting the brain activation of different tasks using solely resting-state data. The prediction quality of the model is dependant on the task (correlation of prediction to actual activation of 0.3 - 0.6) with high levels of significance ($p < 0.001$) for all but one task. The coefficients of individuality and dynamicity are used to train a linear model predicting fluid intelligence. The coefficient of individuality yields the best predictive power (correlation of actual and predicted value of 0.32).

Contents

CHAPTER 1

Introduction

The brain is the most complex human organ and *"has been called the most complex piece of matter in the universe"* [1]. It controls and regulates the activity of the body and is involved in different tasks [1] [2]. The co-activation of multiple cortical areas enables complex cognitive functions like thought processes and emotions [2] [3]. In addition the organization of the brain, its functional connectivity and the correlation to cognitive activity are different for every person and highly individual specific [4] [5]. These problems are addressed in this work and an approach that serves as a possible solution is presented. The main focus of the thesis lies on the calculation of dynamicity of actors as their behaviour of co-activating with different sets of other actors and individuality.

The motivation and aims of the thesis are elaborated in Section 1.1 and the contribution is summarized in Section 1.2. The outline of the thesis is provided in Section 1.3.

1.1 Aims of the Thesis

The human brain is arranged in two cerebral hemispheres which consist of different regions based on distinct features and diverging functions [6]. This organization of anatomical and functional regions is individual-specific and the inter-individual differences are distributed inconsistently across the cortex [6] [7] [8]. Knowledge of this organization is particularly needed for applications in medicine because information on the arrangement of functional regions in the individual subject is required for clinical procedures (e.g. surgical planning and brain stimulation therapy) [6]. Therefore it is a fundamental goal of neuroimaging to get an individual-level parcellation of the cerebral cortex [9].

For this purpose brain functional Magnet Resonance Imaging (fMRI) scans are used as the basis for all calculations. fMRI scans provide information of brain activities in the living human brain [10] [11]. Analysis of this data facilitates research of the connection of anatomy and function and enables the creation of an atlas of brain areas [9]. The idea

is the extraction of all the necessary information from scans at rest as the resting-state activity is robust and the spontaneous fluctuations at rest contain information about functional regions [12] [13]. The networks observed at rest reflect the functional regions of the active brain [14]. The calculation of functional networks from resting-state fMRI data has become a *"standard tool to explore the functional brain organization in neuroscience"* [15].

The goal of this work is the analysis of the human cerebral cortex by creating a parcellation into functionally connected regions. The main focus lies on the research of individuality and dynamicity of the brain and the comparison of the findings with existing state of the art results. In the scope of this work the cortex is parcellated into brain actors on a population level as well as an individual-specific level and this parcellation is used to study the individuality and dynamicity across the cortex. The individualized results are used to create predictive models for different tasks and the fluid intelligence as an example of a cognitive ability linked to brain function.

1.2 Contribution

There are different methods to calculate the brain network delineation (e.g. PCA, ICA) and in this work a novel approach is introduced using Non-negative Matrix Factorization (NMF). The usage of NMF in this context has many benefits because it provides an analysis that is not dependent of the geometry, can be individualized for each subject and also allows inter-subject comparison. Additionally the non-negativity of the results enhances the interpretibility and the dataset is concentrated in two matrices, reducing the dimensionality which increases performance power and usability.

The calculation of the parcellation using NMF as well as the calculation of the coefficients of individuality and dynamicity are summarized in Section 1.2.1. A brief overview of the results is given in Section 1.2.2.

1.2.1 Methods

The calculation of an individualized parcellation consists of three steps:

Step 1. The data matrix containing the complete dataset of all subjects and all subject-scans is factorized using NMF. A high number of iterations results in a clean and distinguished parcellation of n_c regions.

Step 2. The global results from Step 1. are used as an initialisation for a second NMF on the data of each individual subject. The data of a single subject is factorized using the corresponding part of the global result as initial value for the iteration. A predefined stopping criterion prevents over-fitting and results in a parcellation that is comparable to the global results but differs to fit the individual subject.

Step 3. The results from Step 2. have to be mapped to the global results from Step 1. for further use and comparison. This is done using the Hungarian Algorithm [16].

The individualized results are used to calculate the coefficient of individuality by comparing the correlation of the brain regions (brain actors) within the same subject and across different subjects.

The coefficient of dynamicity defined in this work is calculated by comparing the co-activation of the brain actors over the course of time.

1.2.2 Summary of Results

The resulting global parcellation into brain actors is highly reproducible (mean actor correlation $cor = 0.79$ for $n_c = 60$) and the individualized results are highly individual specific (mean within-subject correlation $cor = 0.89$) while maintaining the global structure (mean across-subject correlation $cor = 0.74$).

The individualized results are analysed in regard to individuality and dynamicity. The coefficient of individuality is calculated as the ratio of correlations $r = \frac{within}{across}$ and averaged over the 7 region atlas of [17]. The networks exhibiting the highest individuality are the networks of Ventral-Attention, Fronto-Parietal and Dorsal-Attention while the Limbic, Visual and Motor networks display lower individuality. The coefficient of dynamicity is defined by comparing the co-active actor ids over all time points where the actor is active. An actor that exhibits co-activation with different actors for all time points leads to a higher coefficient of dynamicity compared to an actor that is active with the same group of actors for all time points. The coefficient of dynamicity is averaged over the 7 regions of [17] as well, resulting in high dynamicity in the Visual and Limbic networks (mean values of 0.573 and 0.568) and low dynamicity in the Default network (mean value of 0.459).

The activation during task can be predicted using task-free data. For this purpose a linear model is trained using the actor composition at each point on the cortex as features and task activation maps as targets. The predictive model is functional and provides higher correlation between the predicted activation of a subject with the true activation of the same subject (diagonal) compared to the true activation of all the other subjects (off-diagonal). The diagonal values are significantly different from the off-diagonal values for all tasks but one (Gambling). The tasks yielding the highest quality prediction are Language (mean diagonal correlation $\bar{m}_{ii} = 0.666$) and Working Memory (mean diagonal correlation $\bar{m}_{ii} = 0.660$). The predictive model has the lowest quality for the task Gambling (mean diagonal correlation $\bar{m}_{ii} = 0.147$).

The individuality and dynamicity of the brain actors of an individual subject are connected to cognitive factors like fluid intelligence. This is proven by creating a linear model to predict the value of fluid intelligence of a subject. The correlation of the predicted values of fluid intelligence and the true values is highest when using the coefficient of individuality as the feature of the model ($cor = 0.32$).

1.3 Thesis Outline

In **Chapter 2 State of the Art - Brain fMRI** the most relevant research of brain fMRI analysis is summarized. A brief overview of all the algorithms relevant for the context of this work is given in **Chapter 3 State of the Art - Algorithms**. The methodology used for this thesis is described in **Chapter 4 Methodology** and the experiments that have been conducted are depicted in **Chapter 5 Experiments**. The results and findings are discussed in **Chapter 6 Discussion** and a final conclusion is given in **Chapter 7 Conclusion**. Ultimately following is the bibliography (**Bibliography**).

CHAPTER 2

State of the Art - Brain fMRI

To evaluate the results of this work it is necessary to compare them to existing studies. For this reason the state of the art research is briefly compiled in this chapter. The biological background and histological parcellation methods are explained in Section 2.1. The studies focusing on the calculation of a parcellation into brain networks are summarized in Section 2.2. The publications evaluating a parcellation with the main focus on the research of individuality and the prediction of cognitive activity are recapped in Section 2.3. A brief summary as well as the connection to this thesis are provided in Section 2.4.

2.1 Anatomy and Biology of the Brain

This section serves to provide an overview of the biological viewpoint of brain anatomy and parcellation. The human cerebral cortex has been researched in regard to the cellular structure (cytoarchitecture) and the myelinated fibres (myeloarchitecture).

2.1.1 Cerebral Sulci and Gyri

Ribas [18] summarizes and reviews the literature of the cerebral sulci and gyri to provide a clarified nomenclature of the brain surface areas. In this work 7 brain lobes are defined on each cerebral hemisphere. The neurosurgical definition uses the specific sulci and gyri to explain the exact position. A brief summary of the approximate location of each region is given Figure 2.1 and described below:

1) Frontal Lobe - largest most anterior part of each hemisphere
2) Central Lobe - superolateral surface separated by the central sulcus
3) Parietal Lobe - posterior, adjacent to the central lobe
4) Occipital Lobe - most posterior part of each hemisphere
5) Temporal Lobe - inferior to the Sylvian fissure, superior adjacent to the lobes 1-3,

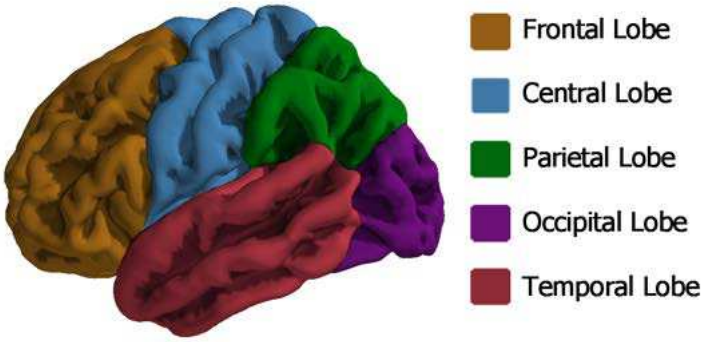

Figure 2.1: Outline of the brain lobes. The approximate location of the brain lobes is visualized in different colours.

posterior adjacent to the occipital lobe
6) Insular Lobe - embedded between frontal and temporal lobes
7) Limbic Lobe - most inferior part of the brain adjacent to the brain stem in the form of a c-shaped ring

The description and interpretation of the results of this work use the nomenclature provided above to describe locations and areas on the cerebral cortex.

2.1.2 Cytoarchitectonic Map of the Human Cerebral Cortex

In the context of cytoarchitectonic brain maps neuroscientists *"have tended to rely almost exclusively on Brodmann's map"* [19]. Brodmann [20] researches the cytoarchitectonics of the cerebral cortex and describes the cellular structure of brain cross-sections as well as its variation across the cortex. This information is used to create a map of 47 brain areas defined by cytoarchitectonic differences. The areas are compared between different mammals (e.g. lemurs and rodents). Von Economo and Koskinas [21] provide the first notes on inter-individual differences of cytoarchitectonic areas [19]. They introduce a more detailed parcellation scheme to create a cytoarchitectonic map differentiating 107 regions [22].

2.1.3 Myeloarchitectonic Map of the Human Frontal Cortex

In contrast to Brodmann, the research of Vogt focuses on the myeloarchitectonics of the human brain. Vogt formulated the first myeloarchitectonic map of the human frontal cortex (published 1910) [23] and is one of the "pioneers of modern neuroscience" [24]. Judas and Cepanec [24] have translated the paper into English.

Vogt creates a brain atlas of 6 regions with multiple subregions each (66 in total) by differentiating the regional variations of three characteristics: *"1) the presence and prominence of individual layers, 2) the number and thickness of myelinated fibres, and 3) the length of radial fibre bundles"* [24].

In addition Vogt provides schematics that display the connection of the myeloarchitectonic layers and the cytoarchitectonic layers.

2.1.4 MRI reflects Myeloarchitecture and Cytoarchitecture

Eickhoff et al. [25] research the connection between lamination patterns of myeloarchitecture, cytoarchitecture and MRI images. For this purpose they focus on two regions of the occipital lobe and compare five imaging modalities including two MRI scans (one in vivo, one post mortem), two myeloarchitectonic staining methods (Heidenhain-Wölke and Black-Gold) and a cytoarchitectonic staining method (Silver cell body stain). They have applied these methods on four different subjects each. The analysis is carried out on regions of interest by calculating a feature vector consisting of 10 parameters. The similarity is quantified by computing the mean Euclidean distance. It is demonstrated that the lamination patterns of the MRI scans reflect the histologic properties and that they are more similar to the myelo- than to the cytoarchitecture. Eickhoff et al. [25] have concluded that MRI scans are dependent on both myelo- and cytoarchitecture with a stronger influence of the myeloarchitecture.

2.2 Parcellation of functional and structural Networks

In this section an abstract of two methods of parcellation in the context of brain MRI data is given.

2.2.1 Clustering of fMRI data

Yeo et al. [17] use functional connectivity MRI and diffusion MRI to estimate cortical organization. For their study the data of 1000 subjects are registered by surface-based alignment. They use a clustering algorithm to combine 1175 uniformly sampled regions of interest with similar functional connectivity profiles. The stability of the clustering algorithm is analysed and used as a criteria for the choice of the number of regions of the parcellation. A parcellation into 7 and 17 regions is calculated and analysed by calculating a confidence map. Additionally the characteristics of the regions are further researched.

The 7 region atlas (see Figure 2.2) is used as a comparison for this work and necessary to enable the comparison of the results of this work with other state of the art results.

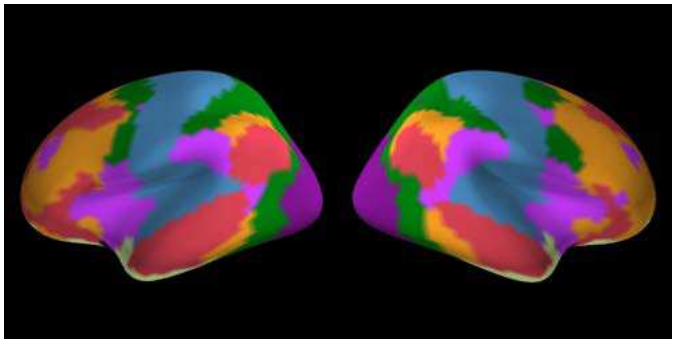

Figure 2.2: Yeo 7 region atlas [17]. The regions are visualized in different colours. The image displays the brain in a lateral view of the left hemisphere (left) and the right hemisphere (right).

2.2.2 Sparse functional networks from rs-fMRI

Li, Satterthwaite and Fan [15] use a non-negative decomposition model on human brain fMRI data to demonstrate the quality of resulting functional networks in comparison to ICA and GIGICA. The main focus of their work lies on the subject specific variation of brain networks. They propose a method that is flexible enough to adapt to the individual while keeping comparability for group-level analysis. This method uses a group sparsity regularization term to enforce common spatial structures as well as a locality regularization term to enhance spatial smoothness. Additionally a parsimonious regularization term is used to avoid large spatial overlap and redundant networks. The optimization model with all the regularization terms yields subject specific networks that are mapped using the Hungarian algorithm [16]. The quality of the parcellation is evaluated with a classification task and a functional coherence measure. The results demonstrate the improvement of quality of the non-negative decomposition model over the widely used methods ICA and GIGICA.

2.3 Individuality

The state of the art research of individual brain parcellation and its application is summarized in this section. The studies compiled in Section 2.3.1, Section 2.3.2, Section 2.3.3 and Section 2.3.4 provide values for comparison with this work regarding the individual specificity of a parcellation by analysing the within- and across-subject variability. Section 2.3.5 and Section 2.3.6 recap the state of the art research focusing on the cognitive activity prediction: the prediction of task activation (Section 2.3.5) and the prediction of fluid intelligence (Section 2.3.6).

2.3.1 Individual specific parcellation

Wang et al. [6] present an approach that starts with a population-based atlas and creates an individual specific parcellation by iteratively amending it using individual subject data. They use a dataset containing 23 subjects, with 5 scans per subject. After applying the iterative method, the results are analysed in regard to intra-subject reproducibility. The calculated mean dice coefficient across the five sessions is 83%. Inter-subject variability is also researched and the mean dice coefficient is 67%. Additionally, the method is tested on another dataset, independent of the one used for algorithm development. This dataset consists of 100 subjects, with 2 scans per subject. The resulting dice coefficients for intra-subject reproducibility (82.4%) and inter-subject variability (60.5%) are similar to the preceding ones. These values are used as a comparison for the results provided in this work.

2.3.2 Individual Variability in Functional Connectivity

Müller et al. [26] study the inter-subject variability of resting-state functional connectivity. The fMRI data used consists of 23 subjects with 5 scans per subject. The resulting inter-subject variability is non-uniformly distributed across the cortex with high values in the lateral prefrontal lobe and the border area of the temporal and parietal lobes. Low values of variability are most notable in the sensory and motor areas. Additionally the functional variability is averaged among specific brain networks (Yeo-7). These results are important for the comparison with the findings of this work.

Furthermore a connection between the individual variability and the evolutionary expansion is assessed and the correlation between functional variability and different brain attributes (e.g. sulcal depth) are researched as well.

2.3.3 Identifying Shared Brain Networks in Individuals by Decoupling Functional and Anatomical Variability

Langs et al. [8] examine resting-state fMRI data of 23 subjects with 5 scans per subject and calculate a functional embedding map to assign regions to the brain vertices based on their functional connectivity. The functional networks are defined by clustering the points in the embedding space and translating back into the anatomical space. The results are individual-specific and the individuality is analysed. The areas demonstrating high individuality are the frontal, parietal and temporal regions whereas the motor, sensory and visual cortices display low individuality. These findings are used for the comparison with the results of this work.

Additionally the method is compared to other state of the art methods and the clinical relevance of the result is discussed as well.

2.3.4 Highly sampled individual human brain

Laumann et al. [27] examine resting-state fMRI data of a single subject and compare their results to group data. The data is parcellated with a resting-state functional connectivity gradient based procedure and the within-subject correlation variability is observerd using the 84 sessions obtained in over more than a year. It is shown that the quality of the parcellation (evaluated by within-subject correlation) is dependent on the number of sessions used. The approximate dependency has the form $1/\sqrt{1+\xi^2}$ with ξ^2 being inversely proportional to the quantity of data. This result is important for the choice of the number of sessions used for the calculations in this work.

The within-subject variability observed is unevenly distributed on the cortex, it is higher in the somato-motoric and visual regions and lower in the medial, fronto-parietal and default mode regions. The results for the across-subject correlation on the contrary demonstrate higher variability in the fronto-parietal and default mode regions with lower variability in the visual and somato-motoric regions. This indicates a high individuality of the former regions. These results are relevant for comparison with the findings of this work.

2.3.5 rs-fMRI predicts task activation

Tavor et al. [28] use functional connectivity at rest to predict individual variations in task responses. They use a HCP dataset consisting of 98 subjects including resting-state measurements, diffusion-weighted MRI and structural MRI. A regression based model in a leave-one-out approach is calculated using 107 predictors and the results are correlated to the true task activations. The prediction quality is measured by comparing the correlations between all the predicted activations and all the true activations. The resulting correlation matrix is diagonal dominant for all but one task (Gambling). These results serve as a comparison for the results in this work.

2.3.6 Functional connectome fingerprinting

Finn et al. [29] research the individuality of activation patterns during rest and tasks of healthy subjects. They use a HCP dataset consisting of 126 subjects and a functional brain atlas with 268 nodes. For each subject a connectivity matrix is calculated by correlating the time courses of each node with the time courses of all other nodes. It is proven that a comparison to a different set of scans of the same subjects allows the identification of individual subjects with a success rate of up to 94.4%. Furthermore it is shown that the most relevant networks for individuality are the medial frontal and the frontoparietal network located in the frontal, temporal and parietal lobes, while the motor and primary visual networks show significantly lower individuality and high consistency across subjects. This is a relevant result for comparison with this work.

The influence on the choice of parcellation, i.e. the number of nodes/networks is researched by using an atlas with 68 nodes and seven networks. The result of this research concludes

that a higher resolution of the parcellation leads to better individual specificity, which is a relevant result for the parameter choice in this work.

Additionally the connectivity profiles are used to predict values of fluid intelligence for the individual subjects using linear regression in a leave-one-out fashion resulting in a correlation score of $r = 0.5$. The most relevant networks for individuality turn out to also be the most relevant for the prediction of this cognitive factor.

2.4 Summary

The human cerebral cortex consists of regions that differ in their cytoarchitecture and/or their myeloarchitecture. These properties are reflected in MRI scans. There is a connection between anatomy and function which is difficult to analyse in the laboratory (e.g. elctromotorcortex can be electrically stimulated). While this has been the only way of research in the past, nowadays MRI scans can visualize the brain activity in the living human brain and the data can be processed by computers.

The calculation of the parcellation into functionally different regions is not trivial and different methods are used for this purpose. It is necessary for the parcellation to be comparable across subject populations as well as individual subjects while being reproducible within the same subject. The method introduced in this work uses the mathematical concept of NMF and is capable of creating a parcellation that is sparse and can be easily interpreted because of the non-negativity of the result.

The individual-specificity is analysed by calculating the intra-subject and inter-subject reproducibility. This way individuality is defined and compared over the cortical surface. This work proposes a method of calculating the coefficient of individuality and it is researched across the cortex.

Brain activation during task performance and cognitive factors like fluid intelligence can be predicted using individualized data. This is proven by predicting task activation using task-free data and predicting values of fluid intelligence using functional connectivity. These experiments are reproduced with the results of this work to showcase the functionality of the methods. In addition the connection between dynamicity, individuality and fluid intelligence is researched.

CHAPTER 3

State of the Art - Algorithms

The algorithms used or referred to in this thesis are introduced in this chapter. The state of the art parcellation methods used are briefly explained first: Principal Component Analysis in Section 3.1 and Independent Component Analysis in Section 3.2. These methods are used in the reference work for the creation of a parcellation of the brain fMRI data. The mathematical basics of the algorithm used for this work is described in Section 3.3 and the specific version used is illustrated in Section 3.4. Sections 3.5 and 3.6 disclose two different methods to fit a linear model and are used in this work for the application and evaluation of the brain parcellation. A brief summary of the state of the art algorithms is given in Section 3.7.

3.1 Principal Component Analysis

The central idea of Principal Component Analysis (PCA) is the reduction of the dimension of a data set into the k main components. For a data vector $\mathbf{x}$ with p variables a principal component is given as a vector $\mathbf{v}_1$ that has maximum variance in the linear function $\mathbf{v}_1^T\mathbf{x}$. The same is done for $\mathbf{v}_2$ uncorrelated to $\mathbf{v}_1$ and this is repeated j-times, with $j = 1, ..., p$. The goal is to find k components that contain most of the variation in $\mathbf{x}$.

The principal components $\mathbf{v}_j$ can be found by solving the eigenvalue problem

$$(C - \lambda I_p)\mathbf{v}_j = 0 \tag{3.1}$$

Where C is the covariance-matrix $C_{ij} = cov[x_i, x_j]$ and I_p the $(p \times p)$ identity matrix. Thus λ is an eigenvalue of C and $\mathbf{v}_j$ the corresponding eigenvector. The derivation and proof are given in [30].

A reconstruction of the data $\tilde{\mathbf{x}}$ using the k most relevant components is calculated as

$$\tilde{\mathbf{x}} = P\mathbf{x} + \bar{\mathbf{x}} \tag{3.2}$$

with the projection matrix $P = \sum_{j}^{k} \mathbf{v}_j \mathbf{v}_j^T$ and the mean of the data $\bar{\mathbf{x}} = mean(\mathbf{x})$.

PCA is a useful tool for the analysis of neuroimaging data [31] that has been applied to fMRI data [31] as well as Positron Emission Tomography (PET) data [32] [33]. In the context of neuroscience PCA is also used to identify neuronal signal spikes and action pontentials [34] [35] [36]. The method of PCA is not limited to the application in the field of neuronal data analysis. It is used in other scientific fields as well and e.g. a common tool for face analysis and facial recognition [37] [38] [39]. The performance and results of PCA are compared to the algorithm of this work explained in Section 3.4 in [40].

3.2 Independent Component Analysis

The main idea of Independent Component Analysis (ICA) is the reconstruction of a mixed signal with independent components. If $\mathbf{x}$ is a vector containing n mixtures of independent components s_j, then each element x_i is defined as

$$x_i = \sum_{j}^{n} a_{ij} s_j \tag{3.3}$$

using the parameters a_{ij}. This can be formulated in matrix notation for the vector $\mathbf{x}$ as

$$\mathbf{x} = A\mathbf{s} \tag{3.4}$$

with the parameter matrix $A = [a_{ij}]$. For the calculation of the independent components the matrix A is estimated and its inverse W is computed. The components $\mathbf{s}$ are calculated as

$$\mathbf{s} = W\mathbf{x} \tag{3.5}$$

A detailed explanation is given in [41].

This method is employed in the works of [13] and [42]. It is used as a comparison in [15] explained in Section 2.2.2. In the context of neuroscience ICA is used for the analysis of electroencephalogram and magnetoencephalogram data as well - especially for the removal of ocular artifacts [43] [44]. In addition to the application in biomedical signal analysis ICA is used in other scientific fields [45] [46] e.g. for the separation of speech mixtures [47] or image de-noising [48]. The algorithm of this work explained in Section 3.4 is i.a. compared to ICA in [40].

3.3 Non-negative Matrix Factorization

The basic idea of Non-negative Matrix Factorization (NMF) is the factorization of a non-negative matrix into two non-negative matrices.

$$X = WH \tag{3.6}$$

The $n \times m$ matrix X is represented by the product of an $n \times n_c$ matrix W and an $n_c \times m$ matrix H, where n_c denotes the number of components. The energy minimization problem that has to be solved is formulated as

$$\begin{aligned} &\min_{W,H} && ||X - WH||^2 \\ &subject\ to && W \geq 0, \quad H \geq 0 \end{aligned} \tag{3.7}$$

The solution of this problem is acquired by applying a multiplicative update following the rules

$$H_{a\mu} \leftarrow H_{a\mu} \frac{(W^T X)_{a\mu}}{(W^T W H)_{a\mu}} \qquad W_{ia} \leftarrow W_{ia} \frac{(X H^T)_{ia}}{(W H H^T)_{ia}} \tag{3.8}$$

A proof of convergence is given in [49].

NMF is used in the research of nuclear medicine for the analysis of PET images [50] [51]. Apart from the application in biomedical signal analysis NMF is employed in astronomical image analysis for pan-sharpening and classification [52] [53] as well as computer vision studies e.g. for facial recognition [54] [55].

This method serves as the basis for the specific method used in this work explained in Section 3.4.

3.4 Orthonormal Projective NMF

Sotiras et al. [40] display the benefit of using NMF on neuroimaging data in regard to interpretibility and adaptability. They introduce the use of Orthonormal Projective Non-negative Matrix Factorization (OPNMF) in the context of brain analysis. The quintessence of OPNMF denotes the load matrix H as the projection

$$H = W^T X \tag{3.9}$$

thereby implicating the reduction of the overlap across the estimated components and the facilitation of high sparsity within the estimated components. The energy minimization problem is therefore remodeled as

$$\begin{aligned} &\min_{W} && ||X - WW^T X||_F^2 \\ &subject\ to && W \geq 0,\ \ W^T W = I \end{aligned} \tag{3.10}$$

with the squared Frobenius norm $||X||_F^2 = trace(X^T X)$ and the identity matrix I. The solution to this problem is calculated iteratively as

$$W'_{ij} = W_{ij} \frac{(XX^T W)_{ij}}{(WW^T XX^T W)_{ij}} \tag{3.11}$$

In the work of Sotiras et al. [40] this algorithm is applied to two different datasets: 1. DT images of mouse brains and 2. human sMR images. The interpretibility of the results is analyzed by calculation of component sparsity and component incoherence. A comparison to two other methods (ICA and PCA) demonstrates the quality and the potential of OPNMF in this field (see Figure 3.1). For this reason this algorithm is adapted for the calculation of this work.

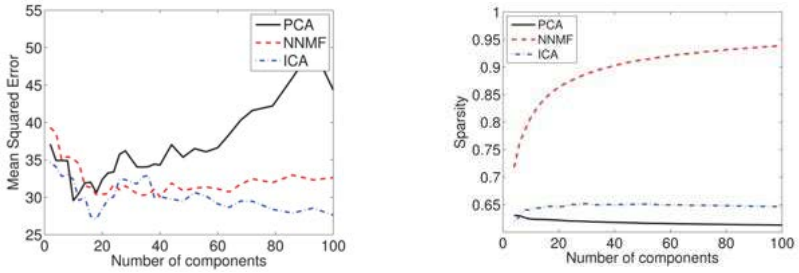

(a) (b)

Figure 3.1: Comparison of the results on the human sMR data set. The mean squared error is plotted in (a) and the component sparsity in (b). The images are taken from [40] with permission from the author.

3.5 Linear Regression

The use of linear regression enables the formation of a linear model that fits target values. The data matrix X contains the individual features x_i for each sample and the targets for the regression are the elements of the vector $\mathbf{y}$. A single target value y is approximated as $\tilde{y}$ in a linear fashion:

$$\tilde{y} = \alpha + \sum_i \beta_i x_i \tag{3.12}$$

with the intercept α, the coefficients β_i and the individual features x_i. To compute the coefficients β_i the ordinary least squares method solves the problem

$$\min_{\beta} ||X\beta - \mathbf{y}||_2^2 \tag{3.13}$$

Linear regression is used in this work to create a linear model capable of predicting the fluid intelligence of an individual subject. This is explained in more detail in Section 4.8.

3.6 Stochastic Gradient Descent

Stochastic Gradient Descent (SGD) is another approach to fit a linear model that is especially useful for a high number of samples (and features) [56]. Similar to (3.12) the training data consists of the features $\mathbf{x_i}$ and targets y_i and the linear approximation $f(\mathbf{x})$ is formulated as:

$$f(\mathbf{x}) = \mathbf{w}^T\mathbf{x} + b \tag{3.14}$$

with the model parameters $\mathbf{w}$ and the intercept b. These parameters are computed by minimizing the regularized training error function $E(\mathbf{w}, b)$.

$$E(\mathbf{w}, b) = \frac{1}{n}\sum_{i=1}^{n} L(y_i, f(\mathbf{x_i})) + \alpha R(\mathbf{w}) \tag{3.15}$$

where $L(y_i, f(\mathbf{x_i}))$ is the loss function and $\alpha R(\mathbf{w})$ is the regularization term. For this work the least squares and the L2 norm are chosen for the loss function and regularization.

This method has advantages over Linear Regression for a high number of samples (and features) and is therefore used in this work to create a linear model for the prediction of task activation. A detailed explanation is given in Section 4.7.

3.7 Summary

There are different parcellation methods and three of them are described. The first one is PCA and calculates the principal components by solving an eigenvalue problem. ICA reconstructs a mixed signal with independent components calculated with a parameter matrix. The third method introduced is used for the calculations of this work: NMF. NMF approximates a non-negative matrix with the product of two non-negative matrices W and H that are iteratively calculated. OPNMF derives H as the projection of W on the original data thereby enhancing the sparsity.

Two methods to fit a linear model are used in this work: 1. linear regression using the ordinary least squares method and 2. SGD which minimizes a regularized training error function. The use of SGD is beneficial for a high number of samples (and features). In this work linear regression is used to predict fluid intelligence and SGD is used to predict task activation.

CHAPTER 4

Methodology

This chapter provides a detailed description of the methodology used in this work. An overview of all the notation is given in Section 4.1 and a definition of the problem is given in Section 4.2. In the following Section 4.3, the usage of NMF is showcased by generating group-level results and the process of individualization is explained in Section 4.4. The individual-specific results contain information about the dynamicity and individuality. The introduction of a coefficient of individuality is given in Section 4.5 and the dynamicity is researched in Section 4.6. Section 4.7 and 4.8 depict the possibility of predictive models using the prior results: Section 4.7 describes the prediction of task activation and Section 4.8 the prediction of fluid intelligence. A brief summary of the methodology is given in Section 4.9.

4.1 Notation

To present a transparent notation throughout the equations of this work the most important features of all of the mathematical objects used are briefly explained below. Further explanation and context is provided in the equations where they are introduced in the following sections.

n	....	Number of points of measurement
m	....	Number of time points
n_c	....	Number of components
m_i	....	Number of time points for a single subject scan
X	....	dataset matrix of all subjects with size $n \times m$
W	....	matrix of all subjects with size $n \times n_c$
H	....	matrix of all subjects with size $n_c \times m$
X_i	....	dataset matrix of individual subject i with size $n \times m_i$
W_i	....	matrix of individual subject i with size $n \times n_c$
H_i	....	matrix of individual subject i with size $n_c \times m_i$
$\boldsymbol{Z}_i$	....	vector of task activation for individual subject i with length n
f_i	....	cognitive data (fluid intelligence) of individual subject i

4.2 Problem Definition

fMRI scans provide information of brain activities in the living human brain [57]. Analysis of this data facilitates research of the connection of anatomy and function and enables the creation of an atlas of brain areas. This organization of anatomical and functional regions is individual-specific and the differences are distributed inconsistently across the cortex [6]. Therefore the algorithm used has to be flexible enough to adapt to the individual while keeping comparability for group-level analysis.
There are different tools and algorithms to calculate a parcellation (e.g. PCA, ICA, NMF). In this work NMF is used because it provides non-negative results that are reproducible and interpretable. In contrast to other techniques that result in positve and negative values (e.g. PCA), the non-negative results are confined without overlap and can be interpreted in the context of brain activations. The parcellation is used to answer the following research questions:

- Does the use of NMF on brain fMRI data yield a parcellation into functional regions?
- What is the optimal number of brain regions and how reproducible are they?
- Can NMF be used on the global brain atlas to create a map of regions that is specific for an individual subject?
- Are there specific differences in the individualized brain actors and can they be quantified by a coefficient of individuality?
- What does the distribution of individuality across the cortex look like and are there areas with lower or higher individuality?
- How can the dynamics of brain actor co-activation be quantified and is it possible to calculate a coefficient of dynamicity?

- What does the distribution of dynamicity across the cortex look like and are there areas with lower or higher dynamicity?
- Can the individualized brain actors (that are task-free) be used to train a linear model capable of predicting task activation of unseen subjects?
- Can the individualized results be used to train a linear model capable of predicting cognitive factors e.g. fluid intelligence of unseen subjects?
- Is there a connection between dynamicity, individuality and fluid intelligence?

4.3 Identifying Actors with NMF

The focus of this work is the analysis of fMRI data. Each scan X_i contains the data of all the points of measurement on the cortex (in this case 5124) at each given point in time over a set duration (1200 time points) for a single subject. It is necessary for the data to be normalised and non-negative, it has to be preprocessed accordingly. For the purpose of this work it is useful to include more than one scan per subject (i.e. 2). The matrices of two scans X_i^1 and X_i^2 are combined to a new matrix X_i^{12} with the size $n \times 2m_i$ and treated like a single scan with twice the amount of time points. To enable a population-level analysis it is necessary to include multiple subjects. Thus the individual subject data X_i^{12} (abbreviated as X_i) are combined to create the data matrix X:

$$X = (X_1 X_2 \cdots X_i \cdots X_s) \ , \tag{4.1}$$

containing the individual scans of all subjects $i = 1, ..., s$ with the number of subjects s. Hence the data matrix X has the size $n \times m$ with the total number of time points $m = s \cdot 2m_i$.

As shown in Section 3.3, the basic idea of NMF is the factorization of a non-negative matrix into two non-negative matrices. In this case the equation is formulated as:

$$X = WH \tag{4.2}$$

The $n \times m$ matrix X is represented by the product of an $n \times n_c$ matrix W and an $n_c \times m$ matrix H, where n_c denotes the number of components (See Figure 4.1). In the context of fMRI analysis, W and H are interpreted as follows:

The non-negative matrix W consists of a set of n_c values per measurement point. The column vectors in W are therefore interpreted as weights on each point of measurement on the brain and form actors $\mathbf{a_j}$, that are interpreted as basis vectors in the functionality space of the brain (see Figure 4.2 for a schematic visualization). This means that all possible brain activities can be reconstructed by a sum of these actors.

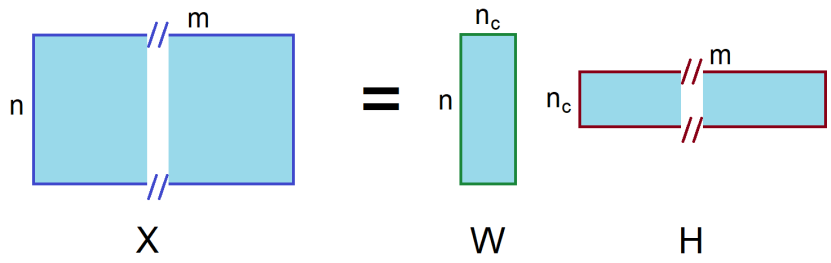

Figure 4.1: Visualization of the matrices involved in the global NMF calculation.

$$W = \begin{pmatrix} | & | & & | & & | \\ \mathbf{a_1} & \mathbf{a_2} & \cdots & \mathbf{a_j} & \cdots & \mathbf{a_{n_c}} \\ | & | & & | & & | \end{pmatrix}, \tag{4.3}$$

with the index $j = 1, ..., n_c$.

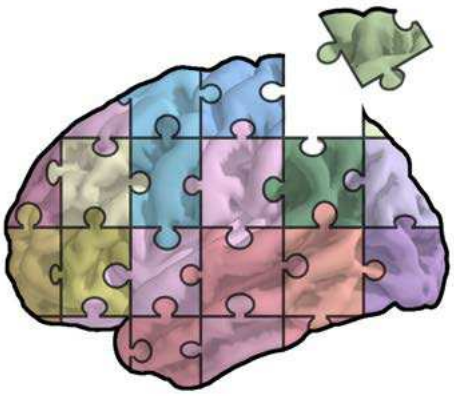

Figure 4.2: Schematic visualization of brain actors.

The non-negative matrix H consists of a set of n_c values for each time point in the measurement. These values are interpreted as weights for the individual actors, therefore columns $\mathbf{h_t}$ contain the information about the co-activation of the actors at a given time point t.

$$H = \begin{pmatrix} | & | & & | & & | \\ \mathbf{h_1} & \mathbf{h_2} & \cdots & \mathbf{h_t} & \cdots & \mathbf{h_m} \\ | & | & & | & & | \end{pmatrix}, \tag{4.4}$$

with the index $t = 1, ..., m$.

The product of one row in W and one column in H is the reconstruction of the original data at a single point of measurement and of time.

To calculate the factorization it is necessary to provide n_c as an input for the algorithm. The value represents the number of resulting brain regions. For the context of this work it is necessary to have the right amount of brain regions and therefore a specific value n_c. The results are used for model calculation hence a higher number increases the dimensionality of the model and the quality of the prediction. The parcellation of the brain signal is aimed to result in functionally and anatomically distinct regions. Thus there is an upper limit of n_c, where regions with the same function are split into multiple parcels (e.g. a split of a symmetric region into two regions for the two hemispheres). This limits the range of n_c; to get the final value used for the calculations in this work, the reproducibility of the result is used as a measure of quality.

In this section the (pre-processed) fMRI data is used to compute the non-negative factorization into two matrices W and H. The original data dimension $n \times m$ is reduced to $n \times n_c$ and $n_c \times m$. The matrix W contains information of the brain actors i.e. connected functional areas while the matrix H encloses the knowledge of their activation in time. The results are called *global* because they include all subjects.

4.4 Individualization

The resulting matrices W and H represent the data of all subjects used for the calculation. To get an individual specific result the NMF algorithm is applied a second time using the global results as an initialisation. This time the data of every single subject X_i is factorized:

$$X_i = W_i H_i \tag{4.5}$$

In this calculation the initialisation for W_i is the global W, and for H_i the submatrix of the global H containing the information related to a single subject (with the size $n_c \times m_i$).

The algorithm approximates the factorization iteratively until a point of convergence is reached. This point is predefined by a stopping criterion. Possible choices for a stopping criterion are the number of iterations or the tolerance of change between iterations. The choice of the correct criterion is not trivial and requires additional research (see Section 5.3.1). This is especially true in this case because the algorithm tends to diverge from the initialisation which is an undesired event in the context of this work.

The resulting matrices W_i have the same dimension and interpretation as the global W from (4.3), while being individual specific. Albeit the latter is true for H_i, the former is not: the information of a single subject is contained in a fraction of all time points, therefore the dimension of H_i is $n_c \times m_i$, with m_i being the time points of the scan for a single subject (See Figure 4.3).

$$H_i = \begin{pmatrix} | & | & & | & & | \\ \mathbf{h_1} & \mathbf{h_2} & \cdots & \mathbf{h_t} & \cdots & \mathbf{h_{m_i}} \\ | & | & & | & & | \end{pmatrix}, \tag{4.6}$$

with the index $t = 1, ..., m_i$.

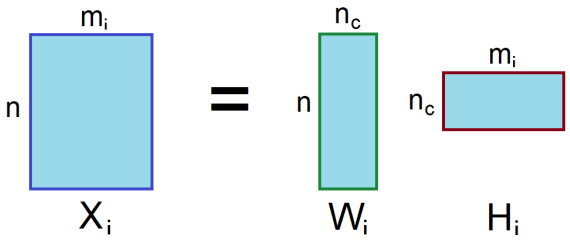

Figure 4.3: Visualization of the matrices involved in the individualization NMF calculation.

The amount of data used for each individual calculation is significantly lower compared to the global calculation, as the second dimension of X_i (and H_i) is only a fraction of the global X (and H). Therefore the algorithm tends to overfit the data by scattering the global brain actors into noisy regions that have no functional or anatomical interpretation. To avoid this effect it is necessary to limit the number of iterations and find a suitable stopping criterion. To this end two values are examined: the within-subject and across-subject correlation. The number of iterations chosen as a stopping criterion has a high ratio of these values while retaining a high difference.

To enable a comparison of the results of different individuals, the W_i and H_i have to be mapped. The Hungarian Algorithm [16] and a Euclidean distance between the individual actors $\mathbf{a_j^{global}}$ and $\mathbf{a_j^{individual}}$ (with $j = 1, ..., n_c$) is used for this purpose. This method allows a comparison of individual subjects, but also of groups of subjects.

In summary the global results W and H are used as an initialisation of a second NMF to compute individual specific results W_i and H_i. These matrices are different for each subject and fitted to the individual characteristics. The individual brain actors maintain the gross structure of the global result and are mapped to them to enable a comparison of different individuals.

4.5 Quantifying Individuality

The within-subject and across-subject correlation can be calculated for each brain actor and compared across the cortex. The correlation of each actor pair a_j, a_k is calculated as

$$within = cor(a_j, a_j) \tag{4.7}$$

$$across = \frac{1}{n_c - 1} \sum_k cor(a_j, a_{k \neq j}) \tag{4.8}$$

for all $j, k = 1, ..., n_c$. This calculation results in one *within* value for each actor, therefore the *across* values are averaged over all $n_c - 1$ co-actors to get one value per actor as well.

There are areas exhibiting correlation across subjects whereas others are specific to each individual subject. This enables the research of individuality by regarding both correlations $within_a$ and $across_a$ of an actor a as well as their ratio r_a given as

$$r_a = \frac{within_a}{across_a} \,. \tag{4.9}$$

The coefficient of individuality $\boldsymbol{r}_i$ is defined as a vector with one entry for each actor specific to an individual subject i.

$$\boldsymbol{r}_i = \begin{pmatrix} r_1 \\ r_2 \\ \vdots \\ r_a \\ \vdots \\ r_{n_c} \end{pmatrix} \tag{4.10}$$

$\boldsymbol{r}_i$ contains the r_a of all actors $a = 1, ..., n_c$ and therefore the complete information of individuality for one individual subject i.

In this section the individualized results W_i are used to define the within- and across-subject correlations and to calculate the coefficient of individuality r_a. A high value of r_a translates to a high value of individuality i.e. an actor that is different across subjects and similar within the same subject. In contrast a low value of r_a indicates that the actor is similar across different subjects and has low individual specificity. The coefficients of a single subject i are compiled into the vector $\mathbf{r}_i$.

4.6 Dynamicity of Actors

Actor activation is dynamic and changes in time. At each point in time different actors are active and have intrinsic patterns of co-activation. A schematic visualization of actor

co-activation patterns is given in Figure 4.4. These patterns are varied: there are actors that stick to a specific pattern of co-activation by being active with the same co-actors for all time points (see Figure 4.4 (b) and (c)) and there are actors that are more dynamic by being part of different patterns of co-activation (see Figure 4.4 (a)).

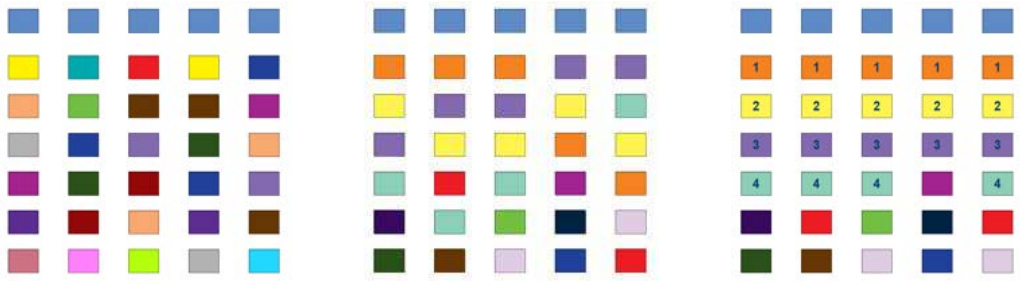

(a) high dynamicity (b) low dynamicity (c) low dynamicity sorted

Figure 4.4: Schematic plot of the actor co-activation. The first row (blue) symbolizes the chosen actor and the other rows below the actors with the highest co-activation. The columns represent different time points. (a) and (b) show the top 6 actors ranked by co-activation strength, (c) displays the co-actors of (b) sorted by actor id.

The dynamicity of actors is estimated by examining the co-activation of the actor with all the other actors at each point in time. This is done via comparison of the entries of $\mathbf{h_t}$ from (4.6) at all time points where the investigated actor is active, i.e. the activation is above a predefined threshold. The threshold is calculated for each actor separately according to the maximum activation of the actor. This way exclusively the time points with in comparison high activation are examined to reduce the number of irrelevant activations due to noise. The assessment of the co-activations allows the calculation of a coefficient of dynamicity for each actor. For one actor a the coefficient of dynamicity is calculated as:

$$c_a^{dyn} = \frac{1}{m_i} \sum_{j}^{m_i} \left(\frac{1}{m_i - j} \sum_{k}^{m_i - j} (1 - o_{jk}) \right) = \frac{2}{m_i(m_i + 1)} \sum_{j}^{m_i} \left(\sum_{k}^{m_i - j} (1 - o_{jk}) \right) , \quad (4.11)$$

with o_{jk} being the overlap between time points j and k, i.e. the fraction of actors with the same id. In this work the top 10% are used (i.e. 6 actors) and therefore o_{jk} can have the values:

$$o_{jk} \in \left[0, \frac{1}{6}, \frac{2}{6}, \frac{3}{6}, \frac{4}{6}, \frac{5}{6}, 1 \right] \quad (4.12)$$

An actor with high values of overlap o_{jk} (e.g. $o_{jk} > \frac{2}{6}$) between multiple time points exhibits low dynamicity c_a^{dyn} because it is active with the same group of actors over

the course of time. If the overlap o_{jk} is low (e.g. $o_{jk} < \frac{2}{6}$) the actor demonstrates co-activation with multiple different actors and therefore higher dynamicity c_a^{dyn}. Thus actors with low c_a^{dyn} display co-activation with specific other actors and exclusively with these actors whereas actors with high c_a^{dyn} exhibit co-activation with (in comparison) many different other actors and change these co-actors during the course of time. This implies that actors with high dynamicity are part of multiple and/or more complex networks compared to the actors with low dynamicity.

The resulting vector of dynamicity of an indvidual subject i is given as $\boldsymbol{c}_i^{dyn}$ defined as

$$\boldsymbol{c}_i^{dyn} = \begin{pmatrix} c_1^{dyn} \\ c_2^{dyn} \\ \vdots \\ c_a^{dyn} \\ \vdots \\ c_{n_c}^{dyn} \end{pmatrix}, \tag{4.13}$$

and contains the c_a^{dyn} of all actors $a = 1, ..., n_c$ and therefore the complete information of dynamicity for one individual subject i.

To summarize, the individualized results H_i are used to define the coefficient of dynamicity c_a^{dyn} by comparison of the actor co-activation and calculating the overlap between time points. If the coefficient of dynamicity is high the actor is co-active with many different other actors whereas an actor with low dynamicity is co-active with the same actors over all (or most) time points. The coefficients of a single subject i are compiled in the vector $\mathbf{c}_i^{dyn}$.

4.7 Predicting Task Activation from Actors

There are two kinds of fMRI scans that differentiate in the activity of the examined subject: 1. resting-state fMRI (subject is at rest) and 2. task fMRI (subject has to perform specific tasks). There is a connection between brain activity at rest and at task activation [28]. Because of this connection the task activation can be predicted using the resting-state data. This means the activation during a specific task is simulated using task-free data.

The activation of tasks is predicted using individual actors matrix W_i (calculated using only data at rest) and their corresponding subject specific task activation maps $\boldsymbol{Z}_i$ (obtained from scans of subjects performing different tasks). A schematic visualization is given in Figure 4.5. The training of the model is done point-wise: the rows of W_i contain the features and the values in $\boldsymbol{Z}_i$ the corresponding targets for a linear regression model. Thus the necessary objects are

$$\boldsymbol{Z}_i = \begin{pmatrix} z_1 \\ z_2 \\ \vdots \\ z_k \\ \vdots \end{pmatrix} \text{ and } W_i = \begin{pmatrix} - & \mathbf{w_1} & - \\ - & \mathbf{w_2} & - \\ & \vdots & \\ - & \mathbf{w_k} & - \\ & \vdots & \end{pmatrix}. \tag{4.14}$$

The row vectors $\mathbf{w_k}$ (i.e. the rows of W_i) contain the actor activation of each actor at the point on the cortex k. This combination of actors is specific for each individual and therefore connected to the corresponding task activation of the same individual. The task activation z_k at the point of measurement k is estimated as

$$z_k = \alpha + \boldsymbol{\beta}\mathbf{w_k}\,, \tag{4.15}$$

with the model parameters α and $\boldsymbol{\beta}$. Since the number of samples is high ($n \cdot$ number of subjects) the SGD algorithm is used to fit the linear model.

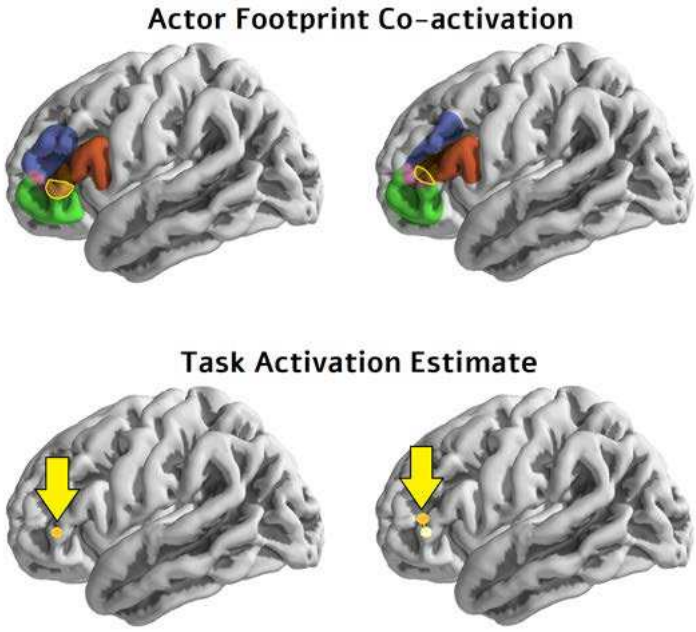

Figure 4.5: Schematic visualization of the task prediction using the resting-state actor footprint co-activation ($\mathbf{w_k}$).

In summary the individualized results W_i and the subject specific task activation maps $\mathbf{Z}_i$ are used to create a linear model to predict the task activation of an unseen subject

using task-free data. For this purpose the SGD algorithm is used in a leave-one-out fashion.

4.8 Predicting Cognitive Data from Actors

The coefficients corresponding to individuality and dynamicity are plausible features for the prediction model of cognitive data. Similar to (4.15) a linear model is trained using the cognitive data f_i as targets and the coefficients $\boldsymbol{c_i}$ as features:

$$f_i = \alpha + \boldsymbol{\beta}\mathbf{c_i} \tag{4.16}$$

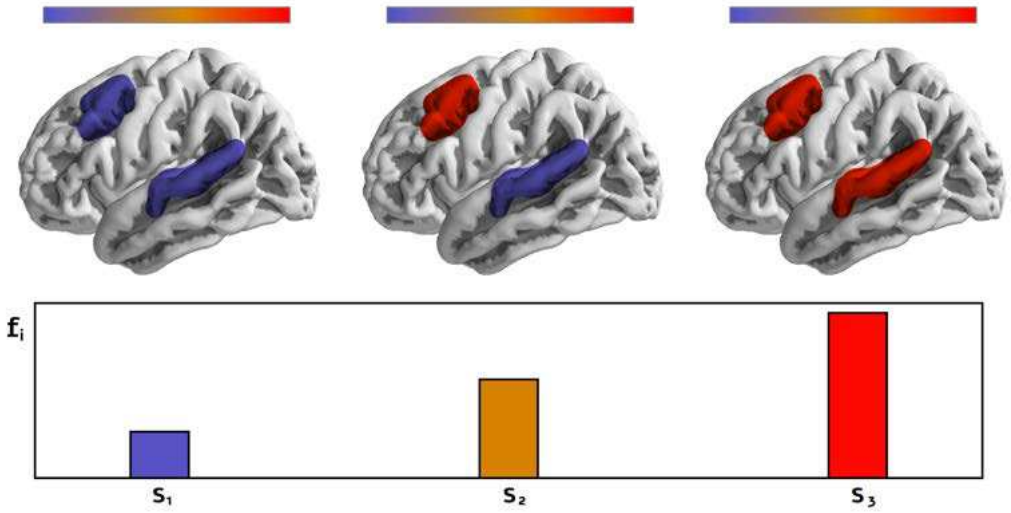

Figure 4.6: Schematic visualization of the cognitive data prediction using the coefficient of dynamicity (value indicated by the colour bar) of the chosen actors (in this case two actors).

In this work the cognitive data is the value of fluid intelligence for each subject. This value is taken from a table of HCP data and has been calculated using Raven's Matrix Test [58]. Two different features are used for model training and prediction:

1. The coefficient of individuality $\boldsymbol{r}_i$ defined by (4.10). In this case the model is formulated as

$$f_i = \alpha + \boldsymbol{\beta}\mathbf{r_i}\,, \tag{4.17}$$

with the fluid intelligence f_i and the coefficient of individuality $\boldsymbol{r}_i$ of the subject i as well as the model parameters α and $\boldsymbol{\beta}$.

2. The coefficient of dynamicity $\boldsymbol{c}_i^{dyn}$ defined by (4.13). The corresponding model is given as

$$f_i = \alpha + \boldsymbol{\beta}\mathbf{c}_i^{dyn}\,, \tag{4.18}$$

with the fluid intelligence f_i and the coefficient of dynamicity $\boldsymbol{c}_i^{dyn}$ of the subject i as well as the model parameters α and $\boldsymbol{\beta}$.

To improve the quality of the model the coefficients of the most relevant actors are determined by calculating the correlation with the cognitive data. A number of k values is selected (with $1 \leq k \leq n_c$) and similar to [29] the values are added up, this way the features $\boldsymbol{c_i}$ are scalars c_i:

$$c_i = \sum_j^k [\mathbf{c_i}]_j \tag{4.19}$$

The values of the actors with the highest correlation are used for a prediction model, the positive feature model f_i^+, and the same is done for the ones with the lowest (negative) correlation, the negative feature model f_i^-.

$$\begin{aligned} f_i^+ &= \alpha + \beta {c_i}^{(+)} \\ f_i^- &= \alpha + \beta {c_i}^{(-)} \end{aligned} \tag{4.20}$$

Here the sign in the exponents indicates the difference in the feature selection for the calculation of c_i. For ${c_i}^{(+)}$ the k highest features and for ${c_i}^{(-)}$ the k lowest features are summed up.

To summarize, the fluid intelligence is used as the prediction target of a linear predictive model. Two different features are used for the model training and prediction: the coefficient of individuality $\mathbf{c}_i^{dyn}$ and the coefficient of dynamicity $\mathbf{r}_i$. For both methods the features are restricted to the most relevant ones, i.e. the ones displaying the highest correlation for the positive feature model f_i^+ and the ones with the lowest correlation for the negative feature model f_i^-.

4.9 Summary

To analyse the activity in the human brain the data of fMRI scans is used for the calculations in this work. For this purpose NMF is employed to create a parcellation into n_c functional brain regions. The combination of the datasets of all subjects enables the calculation of the global matrices W and H. W contains the information of the spatial distribution of the regions on the cortex and the column vectors in W can be interpreted as brain actors. H contains the temporal information and the columns in H comprise the co-activation of the actors.

To calculate individual specific results W_i and H_i for each subject the global W and H are used as an initialisation for a second NMF. The individualized matrices W_i and H_i have the same interpretation as the global matrices W and H. The individual actors are mapped to the global result using the Hungarian Algorithm [16] to enable a comparison of the results.

The individualized brain actors are correlated and the coefficient of individuality $\mathbf{r}_i$ is defined as the ratio of within- and across-subject correlations. The coefficient of dynamicity $\mathbf{c}_i^{dyn}$ is introduced and calculated by comparing the co-activation patterns of brain regions.

The task-free individual specific results can be used to predict task activation. The individualized brain actor composition at each point on the cortex (rows in W_i) are the features and the task activations at each point are the targets for the training of a linear model. After the model training the task activation of an unseen subject can be predicted using the (task-free) brain actor matrix W_i.

To find out if it is possible to predict cognitive data from individualized brain actors, a linear model is trained using the fluid intelligence f_i as targets. Potential features for the model training are the coefficient of individuality $\mathbf{r}_i$ and the coefficient of dynamicity $\mathbf{c}_i^{dyn}$. To enhance the quality of the model the values of each actor are correlated to the values of f_i and the ones demonstrating the highest correlation are selected for the positive feature model while the ones displaying the lowest (negative) correlation are chosen for the negative feature model. After the model training the fluid intelligence of an unseen subject can be predicted using the the selected model feature.

CHAPTER 5

Experiments

The experiments conducted for this work are described in this chapter. First the dataset used is examined in Section 5.1. The application of NMF and the resulting brain parcellation are depicted in Section 5.2. Section 5.3 focuses on the research of individuality and the dynamicity is examined in Section 5.4. The cognitive activity prediction is performed in Section 5.5 in the case of task prediction and in Section 5.6 for the prediction of fluid intelligence. A brief summary of the experiments is given in Section 5.7.

5.1 Dataset

The dataset used is part of the HCP S1200 release [59] and contains 914 subjects with 4 scans per subjects. For this work the dataset is split into two groups for the purpose of stability analysis: *SubjectGroupA* containing the first 453 subjects and *SubjectGroupB* containing the other 461 subjects. To examine the subject stability, the data in *SubjectGroupA* is divided into the *MainDatasetA* and the *ReproductionDatasetA*1 each consisting of two scans per subject. The fMRI data for all subjects includes two different scan methods: scans at rest and while performing tasks. The HCP data itself is preprocessed by the HCP standard preprocessing pipeline [60]. The signals are Gauss-distributed with a mean of zero. To enable the application of NMF the data has to be non-negative. There are two different approaches to enforce this criterion: 1. shift the distribution so that all values are positive and 2. cut off all negative values. For this work method 2 is chosen because it utilises the symmetry of the data distribution and increases the calculation speed.

In addition to the fMRI data the HCP dataset includes a table with supplementary values, one of them is the value for fluid intelligence and is used in this work.

5.2 NMF Results

The regions of the brain parcellation have to be sparse and interpretable. To realize these features the NMF algorithm is applied to the dataset containing all subjects ($MainDatasetA$ or $ReproductionDatasetA1$ respectively). The population-based result fulfils these criteria, which is demonstrated by analysing the actor reproducibility and by comparison of the actor footprints on the cortex with existing state of the art results.

The results for the global NMF are displayed in Section 5.2.1 and the identification of the optimal number of components used for all the calculations is described in Section 5.2.2.

5.2.1 Global Results

To demonstrate that NMF can be used to produce a sparse and interpretable brain parcellation, it is applied on a HCP dataset containing multiple subjects. The resulting population-based atlas can be compared to existing state of the art of brain parcellations and further used to calculate individual-specific results.

The first step in computation of the parcellation is the application of the NMF algorithm on the dataset containing the data of all subjects. The number of components n_c is the one most relevant input parameter. For the following calculations a value of $n_c = 60$ is used, the reason for choosing this specific value is explained in Section 5.2.2. The results for the $MainDatasetA$ and the $ReproductionDatasetA1$ are visualized in Figure 5.1 (a) and Figure 5.1 (b). The correlation of the matching actors is calculated and plotted in Figure 5.1 (c). The mean correlation is 0.789 with a standard deviation (std) of 0.268.

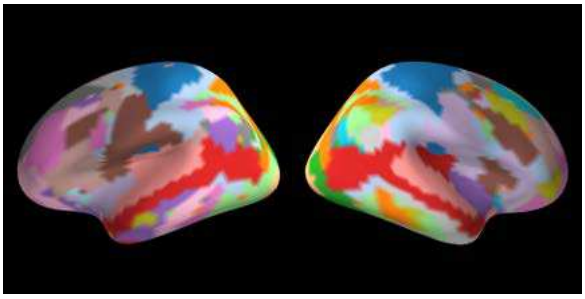

(a) Global actor footprints of *MainDatasetA*

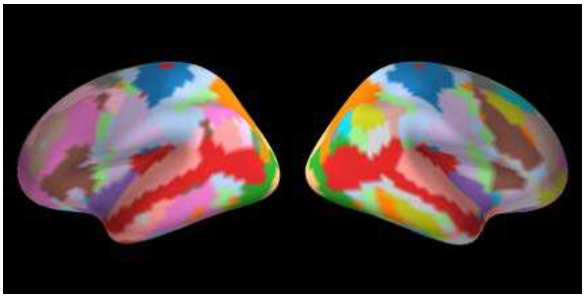

(b) Global actor footprints of *ReproductionDatasetA*1

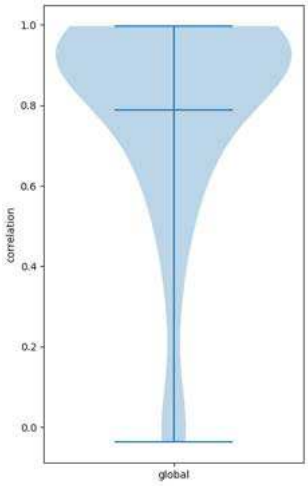

(c) Global actor footprint correlation

Figure 5.1: Winning actor plot of the global result with $n_c = 60$ for two different sets of scans on the same subject group: The *MainDatasetA* in (a) and the *ReproductionDatasetA*1 in (b). The actors are visualized in different colours and only the actor with the highest activation is plotted per point. The images show a lateral view of the left hemisphere (left) and the right hemisphere (right). In (c) the distribution of actor correlation is visualized.

5.2.2 Number of components n_c

As stated in Section 4.3 it is important to find the correct value for n_c. The method is used for both the *MainDatasetA* and the *ReproductionDatasetA*1 to calculate two global results. The resulting actors are mapped using the Hungarian algorithm [16] and the actor correlation is analysed. This is repeated for different values of n_c and the results are compared (see Figure 5.2). The mean actor correlation is high for $n_c = 7$ ($cor = 0.971$) and $n_c = 20$ ($cor = 0.891$). As expected there is a drop in actor correlation for higher values of n_c and the mean for $n_c = 40$ is 0.709, however there is a local maximum for $n_c = 60$ ($cor = 0.789$). The mean values for all tested values of n_c are given in Table 5.1.

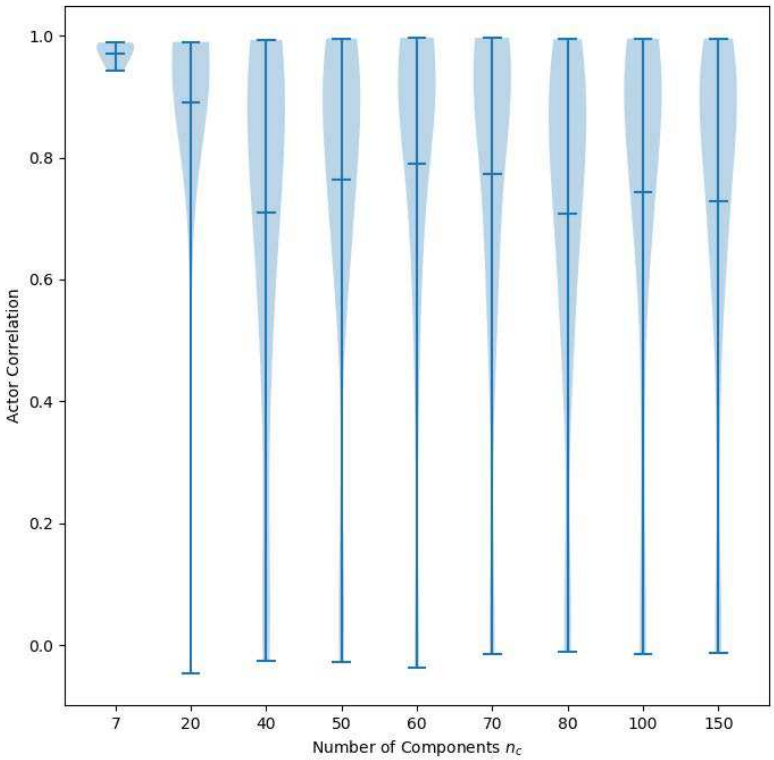

Figure 5.2: Actor correlation of the global NMF results for different n_c.

The global results for $n_c = 7$, $n_c = 60$ and $n_c = 120$ are depicted in Figure 5.3 as winning actor plots. In this plot the cortex is parcellated by visualizing the different actor ids in different colours and each point on the cortex is assigned to the single actor with the highest activation at this point.

n_c	correlation (mean ± std)
7	0.971 ± 0.016
20	0.891 ± 0.224
40	0.709 ± 0.301
50	0.764 ± 0.268
60	0.789 ± 0.268
70	0.773 ± 0.280
80	0.708 ± 0.280
100	0.744 ± 0.293
150	0.728 ± 0.283

Table 5.1: Mean actor correlation of the global parcellation for different values of n_c.

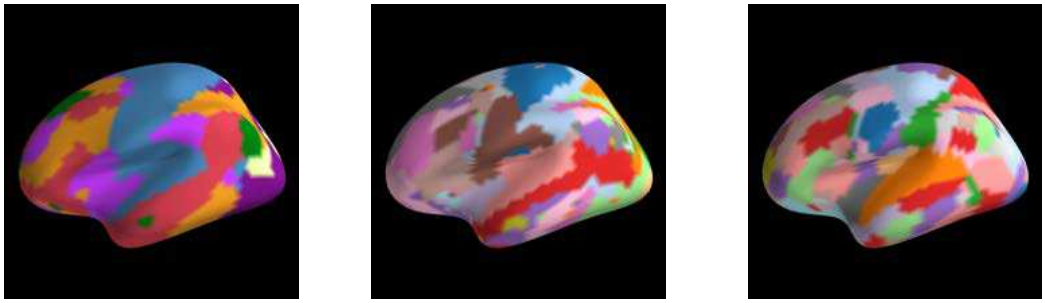

(a) $n_c = 7$ (b) $n_c = 60$ (c) $n_c = 120$

Figure 5.3: Winning actor plot of the global result for different n_c. The actors are visualized in different colours and only the actor with the highest activation is plotted per point. The images show a lateral view of the left hemisphere.

5.3 Individuality

It is a major goal of this work to provide an individual-specific parcellation while retaining group-level comparability. The individualized results have to be reproducible within the same subject and at the same time different across subjects. For this reason a second NMF is performed and the results realize the requirements stated above. This is validated by investigating the within- and across-subject correlation.

An overview of the computation of the individualized results is given in Section 5.3.1. The individualized results demonstrate significant difference when comparing the within-subject and across-subject correlation. This is the requirement for an individual-specific result and examined in Section 5.3.2. The difference is not uniformly distributed across all actors and their footprints on the cortex. To visualize this phenomenon it is imperative to calculate the individuality of the actors. For this purpose a measure of individuality is introduced and visualized in Section 5.3.3.

5.3.1 Individualization

As explained in Section 4.4 the global W and H are used as an initialisation of a second NMF to get individual specific results. For this computation one of the two available scans is used. Hence it can be repeated for the second scan to obtain two individual-specific results per subject. This is relevant to examine the variability within and across subjects. To find the optimal stopping criterion the tolerance of the algorithm is examined as it limits the number of iterations. The quality of the individualization is evaluated by mapping the results and calculating the actor correlation on an intra-subject and inter-subject level. The resulting within-subject and across-subject correlations as well as their difference and ratio are visualized in Figure 5.4 for tolerances between 10^{-1} and 10^{-5}.

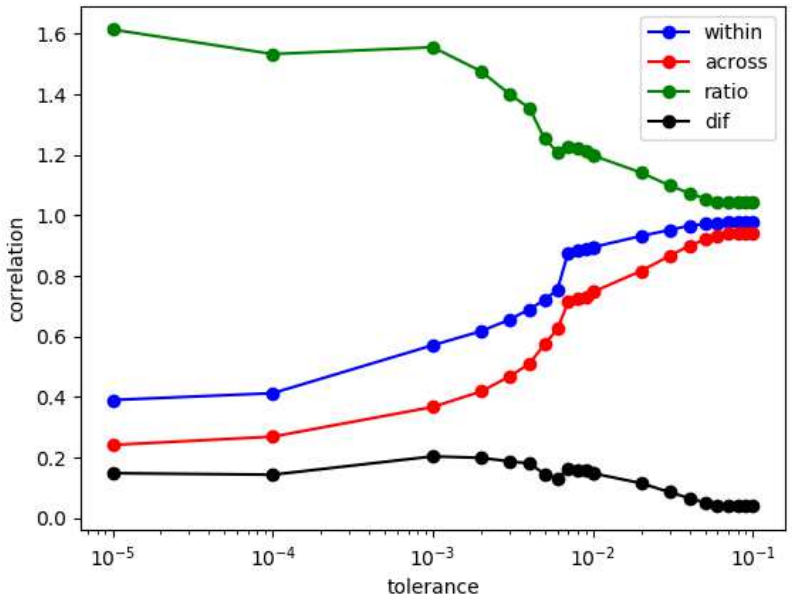

Figure 5.4: Correlation in dependence of tolerance (logarithmic). The mean values of within-subject and across-subject correlations are plotted as well as their ratio $r = \frac{within}{across}$ and their difference $dif = within - across$.

There is a visible drop in quality (i.e. within-subject and across-subject correlation) for tolerances below 10^{-2}. The cause for this drop in quality is a loss of functional and anatomical interpretibility due to scattering of the actor footprints (see Figure 5.5). While the results with a tolerance between 10^{-1} and $8 * 10^{-2}$ are strongly correlated to each other (correlation > 0.8), the results with a tolerance of 10^{-2} show a significant difference for within-subject and across-subject correlation. For this reason the tolerance of 10^{-2} is chosen as a stopping criterion for the individualization.

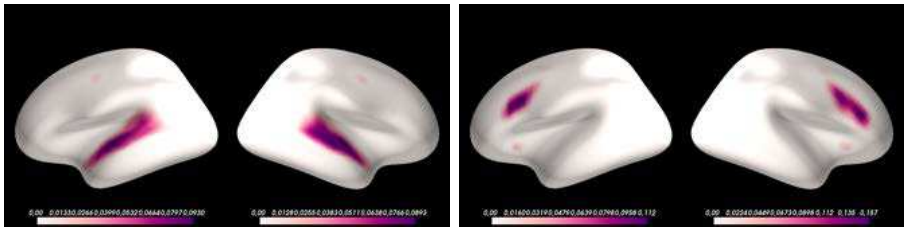

(a) Global actor footprints

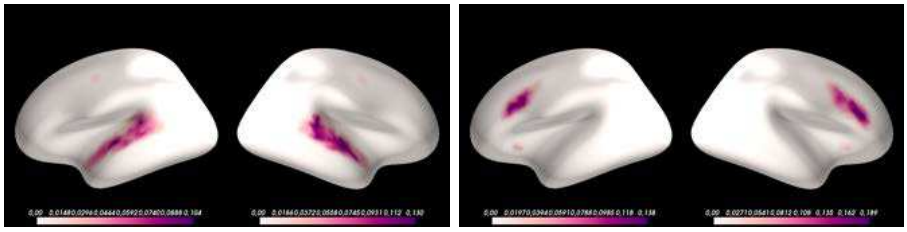

(b) Actor footprints for $tol = 10^{-1}$

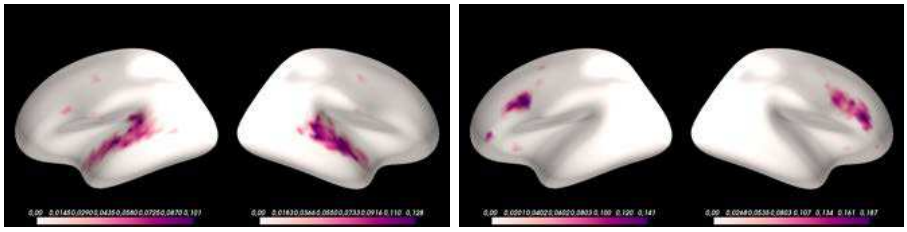

(c) Actor footprints for $tol = 10^{-2}$

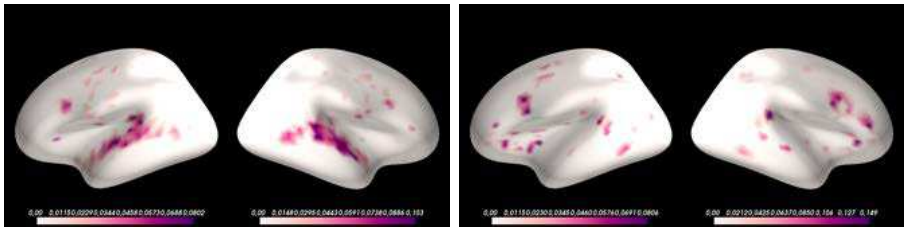

(d) Actor footprints for $tol = 10^{-3}$

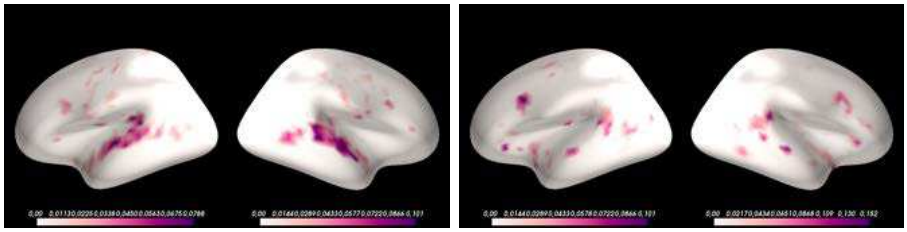

(e) Actor footprints for $tol = 10^{-4}$

Figure 5.5: Actor footprints of two randomly chosen actors for different individualization stopping criteria. Each column shows one actor footprint in a lateral view of the left hemisphere (left) and the right hemisphere (right).

To visualize the individual subject differences four actor footprints are plotted for three subjects and compared to the global actor footprints in Figure 5.6. All of the actors of the individualized result for one subject are plotted in Figure 5.7 (a) for the *MainDatasetA* and for the *ReproductionDatasetA*1 in Figure 5.7 (c) as well as the corresponding actor correlation of matching actors in Figure 5.7 (b) and Figure 5.7 (d). The same plots are given in Figure 5.8 for a different subject. The correlation of matching actors is calculated for both subjects and the mean actor correlation as well as the standard deviation (std) are given in Table 5.2. The values indicate high reproducibility independent of the dataset used. The mean within-subject correlation of the results of the subject in Figure 5.7 is 0.895 for the *MainDatasetA* and 0.890 for the *ReproductionDatasetA*1. The mean actor correlations for the subject plotted in Figure 5.8 are 0.905 for the *MainDatasetA* and 0.906 for the *ReproductionDatasetA*1.

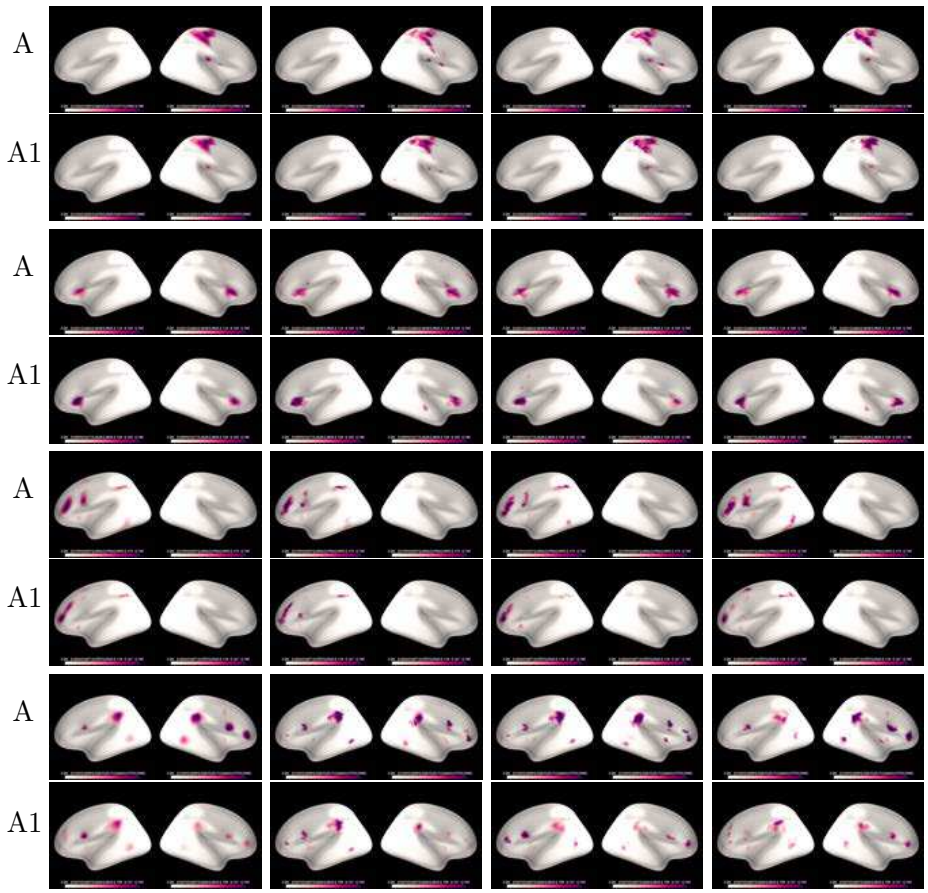

(a) global (b) subject 1 (c) subject 2 (d) subject 3

Figure 5.6: Comparison of actor footprints on the cortex. The same actor is plotted in one row for the global (a) and individualized results of three different subjects (b),(c),(d). The first row shows the results of *MainDatasetA* (A) and the second row the results of *ReproductionDatasetA*1 (A1). Each image displays the lateral view of the left hemisphere (left) and the right hemisphere (right).

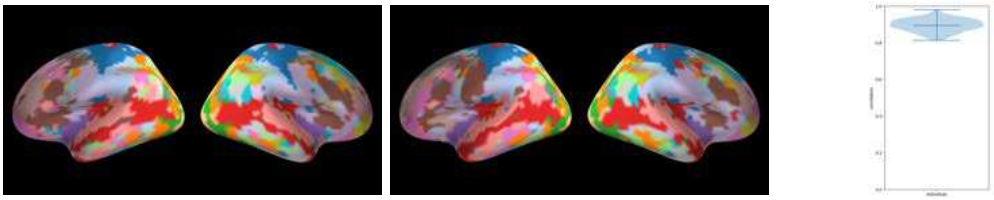

(a) *MainDatasetA* (b)

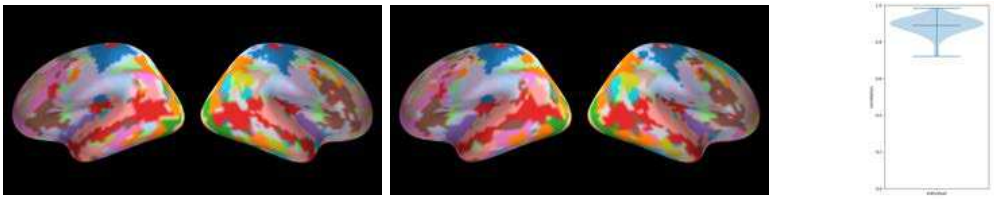

(c) *ReproductionDatasetA*1 (d)

Figure 5.7: Winning actors plot of the individualized results for a single subject. The results for the same subject are visualized for the *MainDatasetA* (a) and the *ReproductionDatasetA*1 (c). For both datasets the results for the first scan (left column) and the second scan (right column) are shown. Each picture shows a winning actor plot in a lateral view of the left hemisphere (left) and the right hemisphere (right). The distribution of correlations of matching actors is shown in (b) for the results of *MainDatasetA* and in (d) for *ReproductionDatasetA*1.

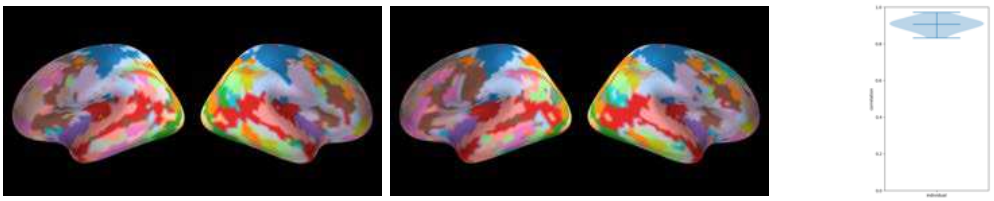

(a) *MainDatasetA* (b)

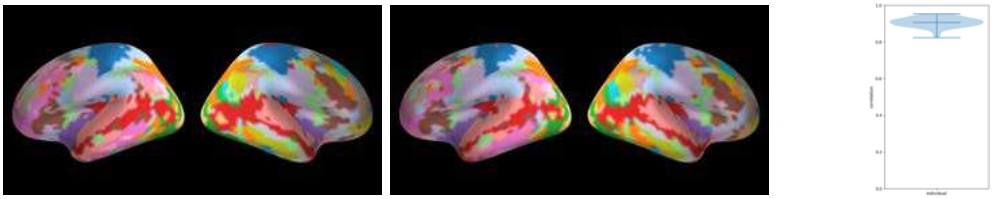

(c) *ReproductionDatasetA*1 (d)

Figure 5.8: Winning actors plot of the individualized results for another single subject. See Figure 5.7.

	correlation (mean ± std)	
	subject 1	subject 2
MainDatasetA	0.895 ± 0.034	0.905 ± 0.034
*ReproductionDatasetA*1	0.890 ± 0.047	0.906 ± 0.026

Table 5.2: Correlation values (mean ± std) of subject 1 (Figure 5.7) and subject 2 (Figure 5.8) for the *MainDatasetA* and the *ReproductionDatasetA*1.

5.3.2 Individual Specificity

To obtain a measure of quality for the individual specificity of the parcellation the within- and across-subject correlation defined by (4.7) and (4.8) are calculated. For each correlation value 1000 randomly chosen subject-couples are selected and the correlation of each actor is determined. This way for each actor 1000 values are measured for both within- and across subject correlation. The distribution of the results is visualized in Figure 5.9.

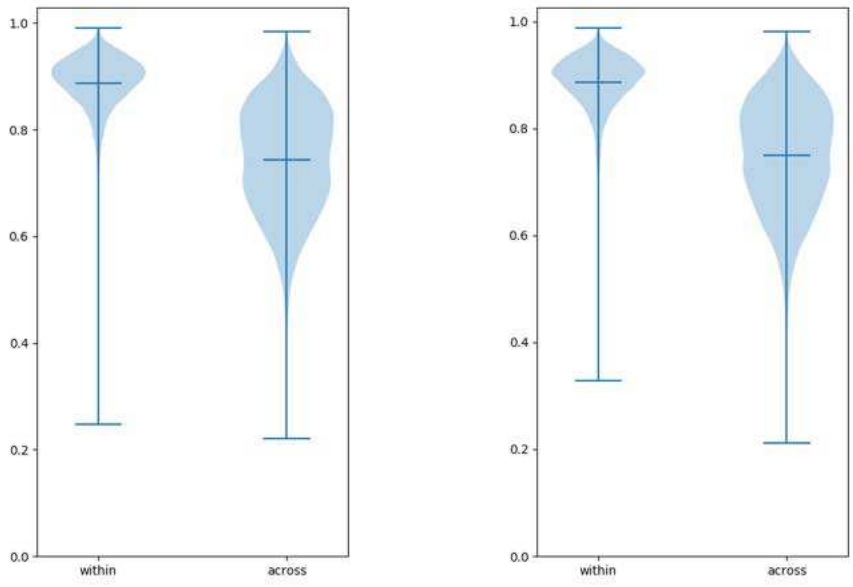

(a) *MainDatasetA* (b) *ReproductionDatasetA*1

Figure 5.9: Distribution of the within-subject and across-subject correlation for the *MainDatasetA* (a) and the *ReproductionDatasetA*1 (b).

The actors for an individual subject have to be significantly different from the actors of another subject to be individualized. An unpaired two-tailed t-test is performed to check if there is a significant difference. The statistical values are given in Table 5.3. The significance of the difference between within- and across-subject correlation is evident: The within-subject correlation is significantly higher than the across-subject correlation. The calculated values for the within-subject correlation are 0.887 for $MainDatasetA$ and 0.885 for $ReproductionDatasetA1$ while the mean across-subject correlation is 0.742 for $MainDatasetA$ and 0.749 for $ReproductionDatasetA1$. The difference is significant for $p < 0.001$ independent of the dataset used.

$MainDatasetA$

within-subject (mean ± std)	across-subject (mean ± std)	t (p)
0.887 ± 0.055	0.742 ± 0.103	302 (p<0.001)

$ReproductionDatasetA1$

within-subject (mean ± std)	across-subject (mean ± std)	t (p)
0.885 ± 0.053	0.749 ± 0.102	290 (p<0.001)

Table 5.3: Statistic values for the within- and across-subject correlations. The t and p values correspond to an unpaired two-tailed t-test applied on the distributions of the within- and across-subject correlations.

5.3.3 Variation in Individuality across the Cortex

While being different for each individual subject, the actors still share the properties of the global initialisation. However the across-subject correlation is more variable (standard deviation $\sigma = 0.1$ compared to the within-subject correlation ($\sigma = 0.05$). Consequently there are actors with higher correlation (> 0.8) and actors with lower correlation (< 0.7), or put in other words: actors that are similar for all subjects and actors that are more individual-specific. To visualize this variation, the ratio $r = \frac{within}{across}$ is calculated and serves as a measure for individuality. The mean over all subjects is plotted in Figure 5.10 as a weighted plot. The values for this ratio are greater than or equal to 1. Where $r = 1$ indicates low (no) individuality ($within = across$) and values $r > 1$ indicate more individual-specificity ($within \neq across$, or rather: $within > across$).

The reproducibility of the result is analysed by calculating the correlation of the results of $MainDatasetA$ an $ReproductionDatasetA1$. The calculated correlation is $cor = 0.894$ which indicates high reproducibility and stability of the result.

The individuality across the cortex is averaged over the 7 Yeo networks of [17]. The regions are plotted in Figure 5.11 (a) and the mean individuality per network is depicted in the bar plot of Figure 5.11 (b). The values are given in Table 5.4. The region exhibiting the highest individuality is the network of Visual Attention with a mean value of 1.250 while the regions with the lowest individuality are the Visual (1.196) and Limbic (1.186)

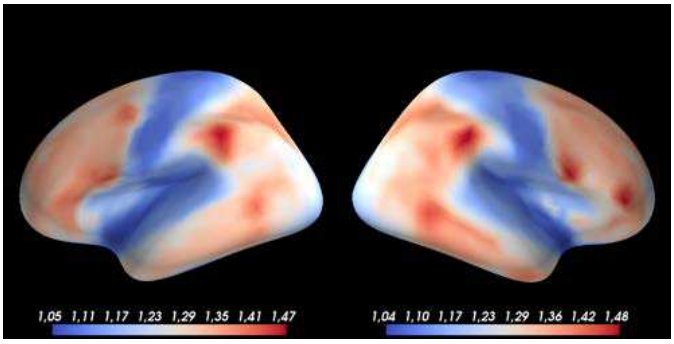

(a) *MainDatasetA*

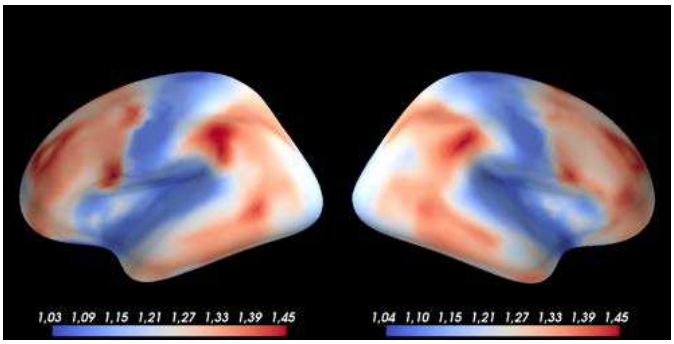

(b) *ReproductionDatasetA*1

Figure 5.10: Individuality plot for (a) the *MainDatasetA* and (b) the *ReproductionDatasetA*1. The ratio of the correlations $r = \frac{within}{across}$ for each actor is weighted by the actor activation at each point on the cortex. The images show a lateral view of the left hemisphere (left) and the right hemisphere (right).

networks. The distributions of the individuality across the 7 Yeo regions are plotted in Figure 5.12 to visualize the spread of the values that is caused by the comparatively big regions that span over areas of low and high individuality.

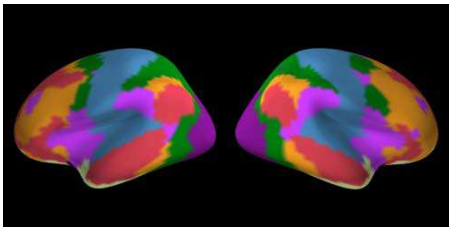

(a) Yeo Regions

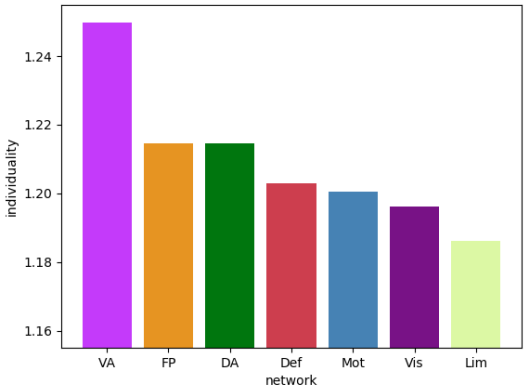

(b) Individuality

Figure 5.11: Individuality of the *MainDatasetA* averaged over the 7 Yeo regions. The regions are visualized on the cortex in (a) and the mean individuality per region is plotted in (b). The regions are defined as 7 networks: Ventral-Attention (VA), Fronto-Parietal (FP), Dorsal-Attention (DA), Default (Def), Motor (Mot), Visual (Vis) and Limbic (Lim).

Network	Coefficient of individuality (mean ± std)
VA	1.250 ± 0.098
FP	1.214 ± 0.107
DA	1.214 ± 0.100
Def	1.203 ± 0.098
Mot	1.200 ± 0.100
Vis	1.196 ± 0.109
Lim	1.186 ± 0.103

Table 5.4: Coefficients of individuality averaged over the 7 Yeo regions.

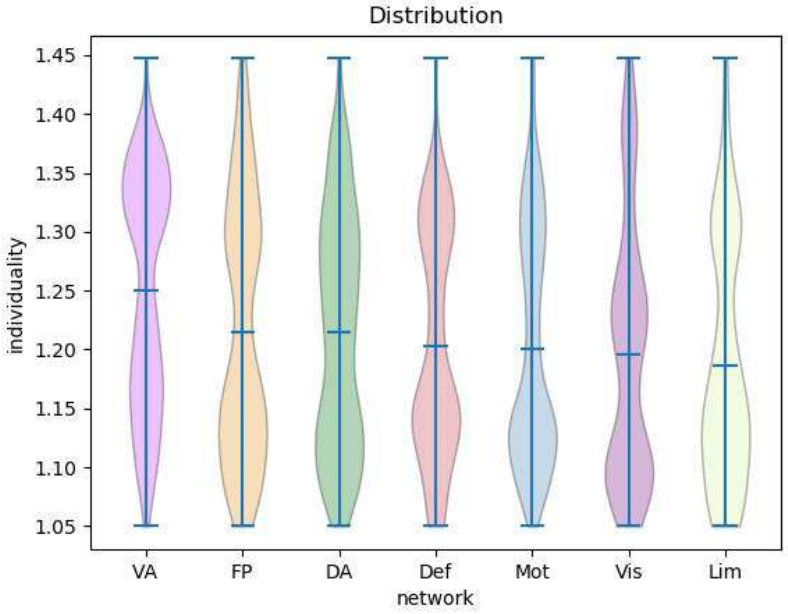

Figure 5.12: Distribution of the coefficient of individuality in each Yeo network.

5.4 Dynamicity & Co-Activation

As explained in Section 4.6, the actor co-activation at each point of time is examined to estimate the dynamicity of the actor. The columns in the matrices H_i contain the activation strength of each actor at a given time. For each actor the time points where the actor is active (i.e. above a threshold) are selected and the co-activation of the other actors is examined. To calculate a coefficient of dynamicity, the top 6 actor-ids (10%) of the co-actors are compared and the fraction of overlap is averaged over all time points. The mean over all subjects is visualized as a weighted plot in Figure 5.13.

The dynamicity across the cortex is averaged over the 7 Yeo regions [17] and the mean values are depicted in a bar plot in Figure 5.14. The specifc values of the mean of each network and their standard deviation are given in Table 5.5. The Visual and Limbic networks demonstrate the highest values of dynamicity (0.573 and 0.568) while the Default network displays the lowest value of dynamicity (0.459). The distribution of the dynamicity across these networks is plotted in Figure 5.15. Similar to the previous results (Figure 5.12) the regions span areas with high and low values of dynamicity.

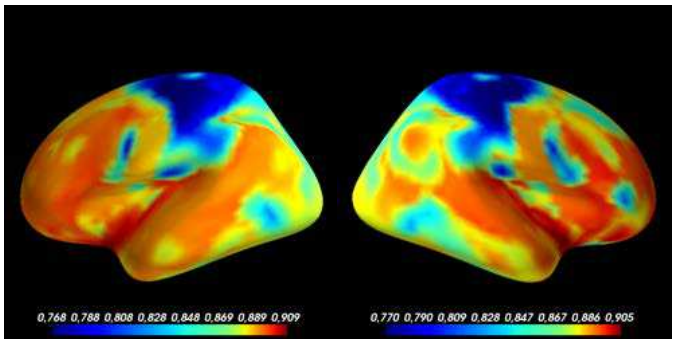

Figure 5.13: Dynamicity averaged over all subjects of the *MainDatasetA*. The dynamicity of each actor is weighted by the global actor activation at each point on the cortex. The images show a lateral view of the left hemisphere (left) and the right hemisphere (right).

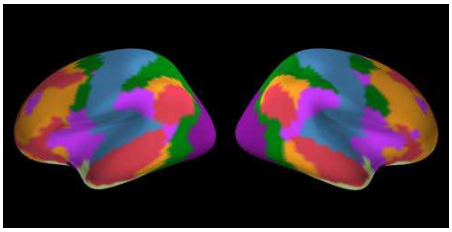

(a) Yeo Regions

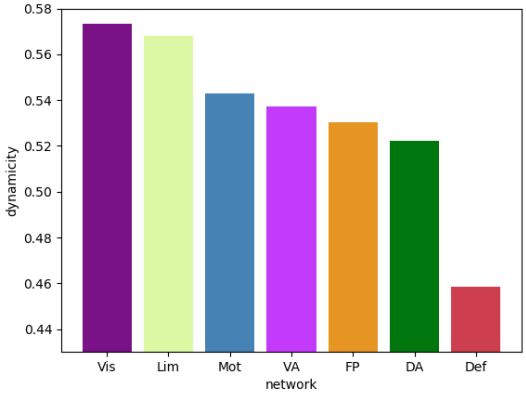

(b) Dynamicity

Figure 5.14: Dynamicity of the *MainDatasetA* averaged over the 7 Yeo regions. The regions are visualized on the cortex in (a) and the mean dynamicity per region is plotted in (b). The regions are defined as 7 networks: Visual (Vis), Limbic (Lim), Motor (Mot), Ventral-Attention (VA), Fronto-Parietal (FP), Dorsal-Attention (DA) and Default (Def).

Network	Coefficient of dynamicity (mean ± std)
Vis	0.573 ± 0.359
Lim	0.568 ± 0.343
Mot	0.543 ± 0.365
VA	0.537 ± 0.355
FP	0.531 ± 0.354
DA	0.522 ± 0.357
Def	0.459 ± 0.382

Table 5.5: Coefficients of dynamicity averaged over the 7 Yeo regions.

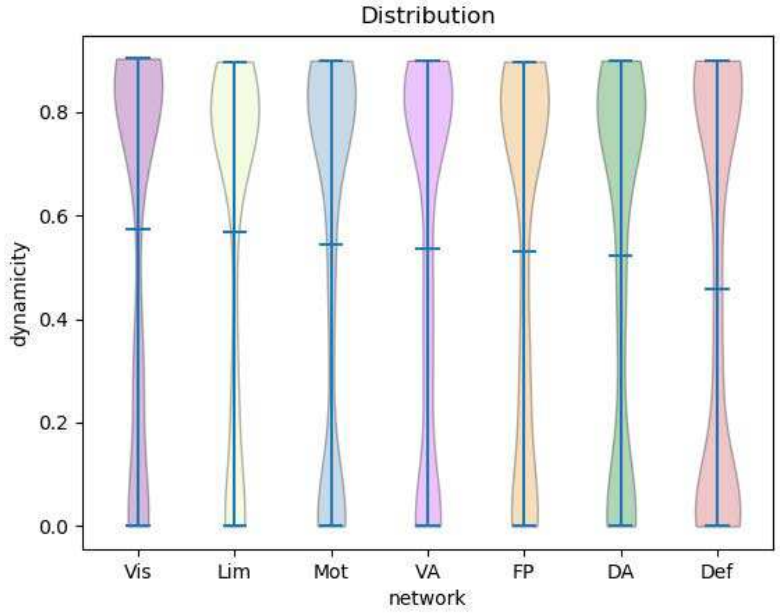

Figure 5.15: Distribution of the coefficient of dynamicity in each Yeo network.

5.5 Task Prediction

As explained in Section 4.7, the individual W_i can be used to predict the task activation $\mathbf{Z}_i$. A linear model is trained and tested in a leave-one-out fashion over all subjects. To evaluate the quality of the model, the predicted activations for each subject and the true activations are correlated to each other, resulting in the matrix of correlations $M = [m_{ij}]$. Where $m_{ij} = cor(true_i, predict_j)$ with the continuous indices i, j that go through all the subjects in the dataset used ($1 \leq i, j \leq 453$ for $MainDatasetA$).

This matrix is normalized for the values in the diagonal ($m_{ii} = 1$) to enhance the quality of the visualization. The correlation of the following plots is colour coded using the colour map shown in Figure 5.16 (c). A comparison of the normalized and not normalized matrix plots for one task (Language 3) is given in Figure 5.16 (a) and (b).

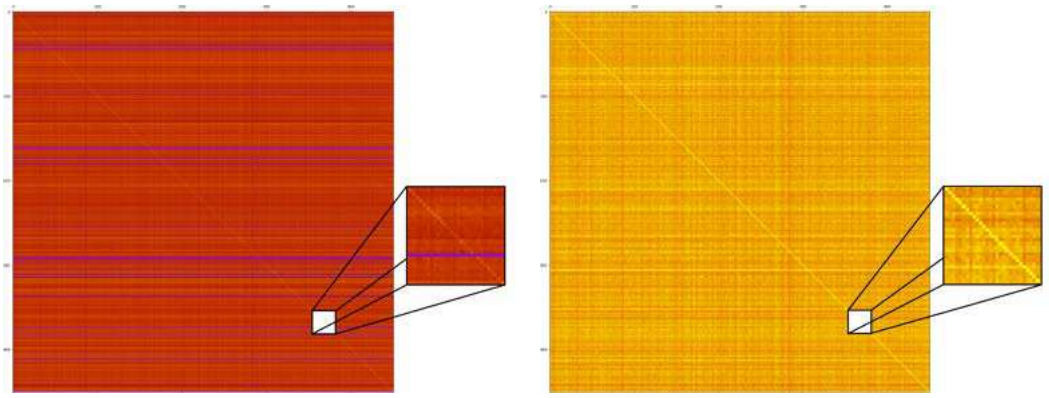

(a) not normalized

(b) normalized

(c) colour map

Figure 5.16: Comparison of the correlation matrix (a) and the normalized matrix (b) for the task Language 3. A small area is magnified to enhance the visibility of the diagonal and highlight the difference to the off-diagonal values, especially in the normalized plot. The colour map used for the visualization of the correlation matrices is given in (c). The warmer colours indicate high correlation whereas the cooler colours indicate lower correlation.

The results for six other tasks are plotted in Figure 5.17 (not normalized) and Figure 5.18 (normalized).

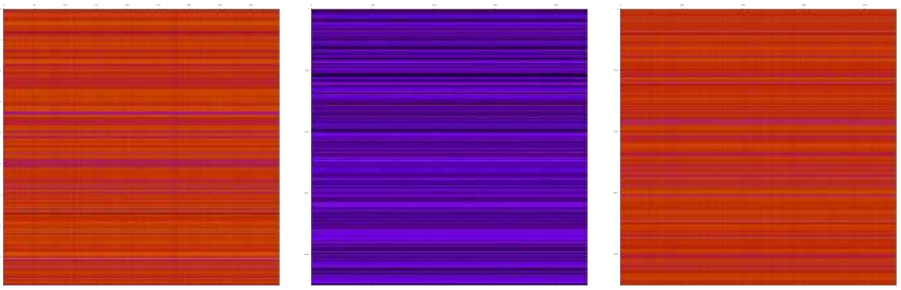

(a) Emotion 3 (b) Gambling 2 (c) Motor 7

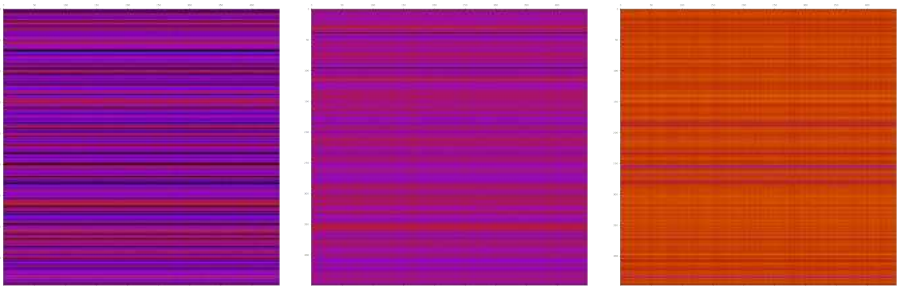

(d) Relational 2 (e) Social 2 (f) WM 9

Figure 5.17: Correlation matrices for different tasks.

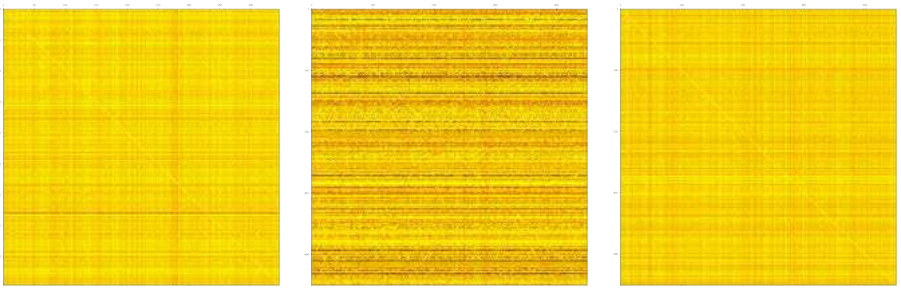

(a) Emotion 3 (b) Gambling 2 (c) Motor 7

(d) Relational 2 (e) Social 2 (f) WM 9

Figure 5.18: Normalized correlation matrices for different tasks.

The values in the diagonal hold the information about the correlation of the predicted and true activation of the same subject. The difference between the diagonal (m_{ii}) and the off-diagonal values ($m_{i\neq j}$) is a measure of quality for the model. To evaluate if there is a significant difference between these values, a two-tailed t-test is performed. The mean values for both the diagonal ($\bar{m}_{ii}$) and the off-diagonal ($\bar{m}_{i\neq j}$) as well as the test results are given in Table 5.6. The mean values of the diagonal are $\bar{m}_{ii} = 0.666$ for the task Language 3 and $\bar{m}_{ii} = 0.660$ for the task WM 9. Their corresponding mean values of the off-diagonal are $\bar{m}_{i\neq j} = 0.576$ (Language 3) and $\bar{m}_{i\neq j} = 0.621$ (WM 9). The difference has the highest significance for these two tasks with $t = 23.6$ (Language 3) and $t = 10.6$ (WM 9). The results for the tasks Motor 7 and Emotion 3 are similar but show less significance in the difference (see Table 5.6). It has to be noted that the difference is still significant for $p < 0.001$. The same is true for the tasks Social 2 and Relational 2 however the mean values of the diagonal $\bar{m}_{ii}$ and off-diagonal $\bar{m}_{i\neq j}$ are lower in comparison. Gambling 2 is the only task with a lower significance of the difference between diagonal and off-diagonal with a critical value of $p = 0.043$ in contrast to the $p < 0.001$ for all the other tasks. Additionally the mean values ($\bar{m}_{ii} = 0.147$ and $\bar{m}_{i\neq j} = 0.135$) are low and have high standard deviations in comparison (0.119 and 0.110). The distributions of the diagonal and off-diagonal values are visualized in Figure 5.19 and for the normalized correlation matrices in Figure 5.20.

	$\bar{m}_{ii}$ (mean ± std)	$\bar{m}_{i\neq j}$ (mean ± std)	t(p)
Emotion 3	0.608 ± 0.104	0.572 ± 0.099	7.3 (p<0.001)
Gambling 2	0.147 ± 0.119	0.135 ± 0.110	2.0 (p=0.043)
Language 3	0.666 ± 0.081	0.576 ± 0.071	23.6 (p<0.001)
Motor 7	0.608 ± 0.086	0.567 ± 0.082	10.1 (p<0.001)
Relational 2	0.332 ± 0.194	0.297 ± 0.179	3.8 (p<0.001)
Social 2	0.437 ± 0.101	0.394 ± 0.092	8.9 (p<0.001)
WM 9	0.660 ± 0.078	0.621 ± 0.075	10.6 (p<0.001)

Table 5.6: Mean values of the diagonal ($\bar{m}_{ii}$) and the off-diagonal ($\bar{m}_{i\neq j}$) and their respective standard deviation as well as the test results of a two-tailed t-test for the different tasks.

For the discussion and interpretation of these results it is relevant to examine the task activation on the cortex. The true and predicted task activations of four different tasks are plotted for a single subject in Figure 5.21.

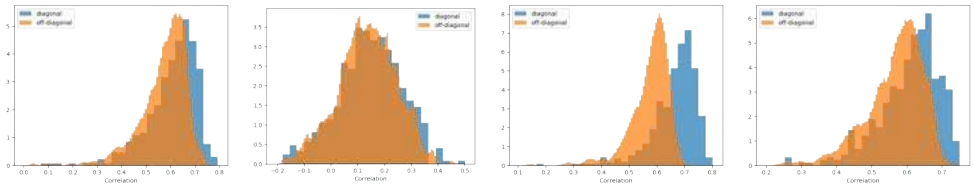

(a) Emotion 3 (b) Gambling 2 (c) Language 3 (d) Motor 7

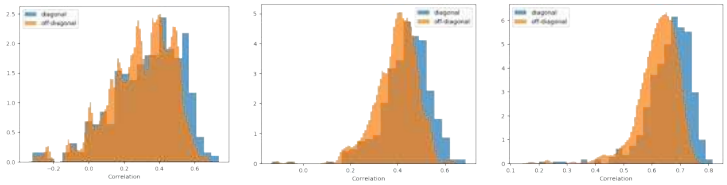

(e) Relational 2 (f) Social 2 (g) WM 9

Figure 5.19: Histogram plots of the diagonal (blue) and off-diagonal (orange) correlation values for each task.

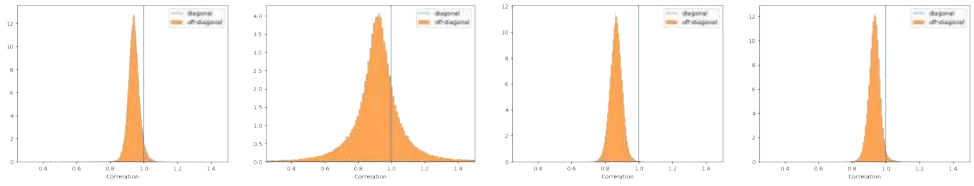

(a) Emotion 3 (b) Gambling 2 (c) Language 3 (d) Motor 7

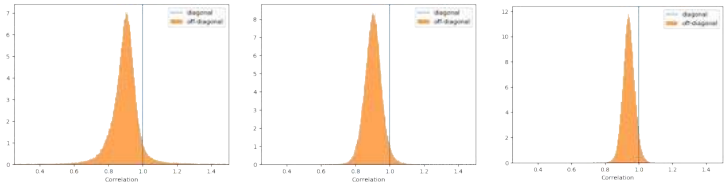

(e) Relational 2 (f) Social 2 (g) WM 9

Figure 5.20: Histogram plots of the diagonal (blue) and off-diagonal (orange) normalized correlation values for each task.

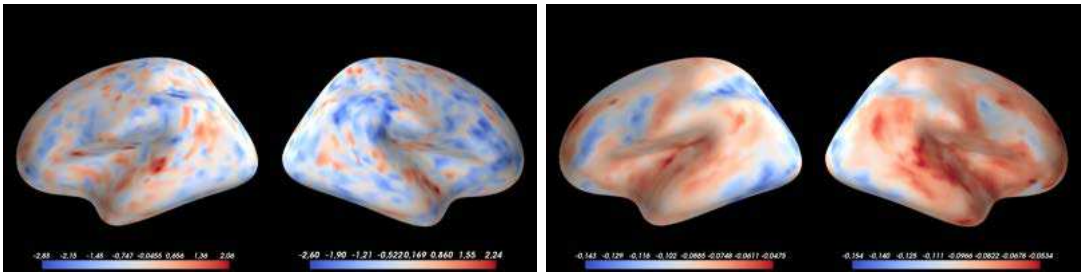

(a) Gambling 2

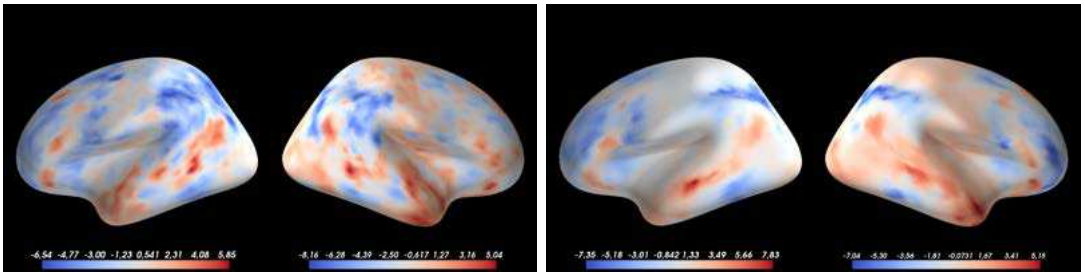

(b) Language 3

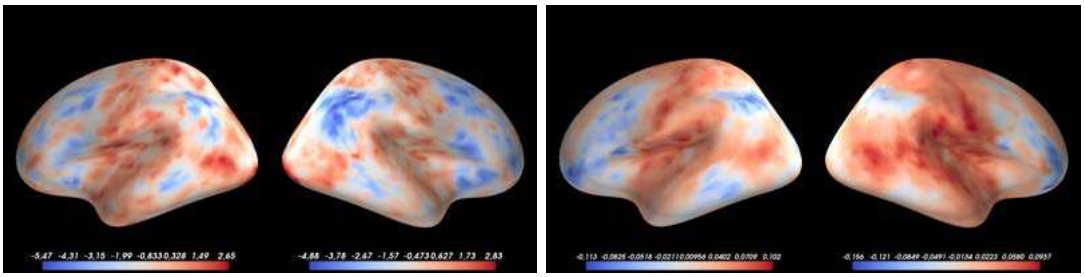

(c) Relational 2

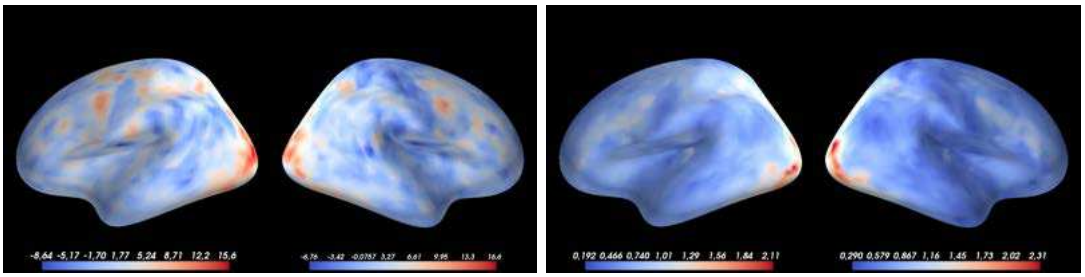

(d) WM 9

Figure 5.21: Comparison of the true task activation (left column) and the predicted task activation (right column) of a randomly chosen subject. Each picture shows the cortex in a lateral view of the left hemisphere (left) and the right hemisphere (right).

5.6 Fluid Intelligence Prediction

The coefficients of dynamicity and individuality include information of cognitive data. As such they can be used to predict the fluid intelligence of an individual. For this purpose a linear model is used according to Section 4.8. To enable a legitimate comparison to the state of the art, a subset of 118 subjects is used. The model is trained and tested in a leave-one-out fashion for different features. Three different features are used: 1. the coefficient of individuality r, 2. the across-subject correlation and 3. the coefficient of dynamicity c^{dyn}. The resulting predicted values of fluid intelligence are plotted in Figure 5.22 and the quality of the prediction is analysed by comparing the true and predicted values in Figure 5.23.

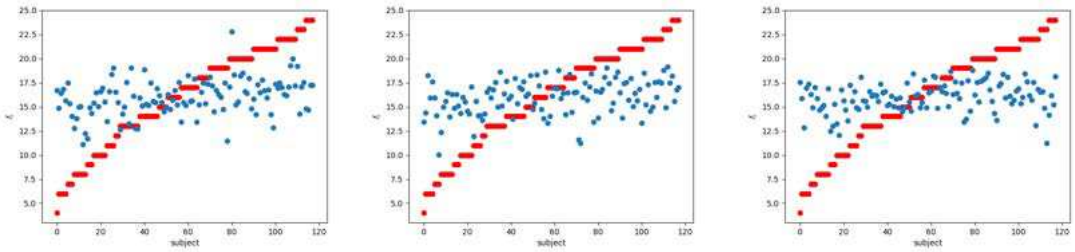

(a) coefficient of individuality (b) across-subject correlation (c) coefficient of dynamicity

Figure 5.22: Fluid intelligence plot. For each subject (x-axis) the affiliated fluid intelligence values are given (y-axis). The true values (red) of all subjects used are sorted and compared to their corresponding predicted values (blue). The predicted values for (a) are the results of the negative feature model f_i^-, (b) and (c) are the values of the positive feature model f_i^+.

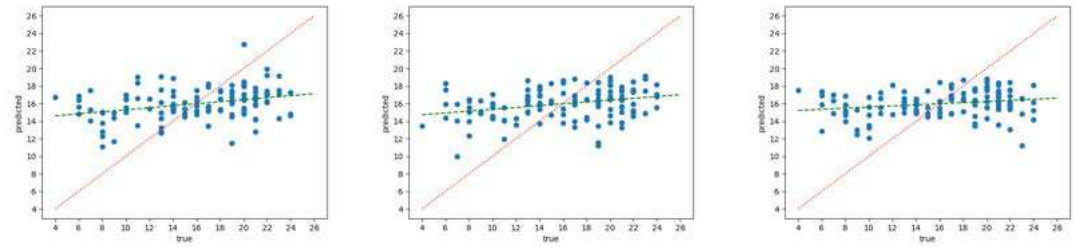

(a) coefficient of individuality (b) across-subject correlation (c) coefficient of dynamicity

Figure 5.23: Prediction quality plot. The predicted values are plotted against the true values. In addition the diagonal (red) and the linear approximation of the scattered points (green) are given. The predicted values for (a) are the results of the negative feature model f_i^-, (b) and (c) are the values of the positive feature model f_i^+.

The correlation of the true and the predicted values is calculated for each result and given in Table 5.7. The best results are obtained by using the coefficient of individuality as the model feature. The correlation of the true and predicted values for the negative feature model is 0.320; the result for the negative feature model is 0.043. The resulting correlation of the positive feature model for the other two features used are 0.301 (across-subject correlation) and 0.218 (coefficient of dynamicity). Here the results for the negative feature model are lower (0.176 and 0.081).

feature of linear model	correlation f_i^+	f_i^-
coefficient of individuality	0.043	0.320
across-subject correlation	0.301	0.176
coefficient of dynamicity	0.218	0.081

Table 5.7: Correlation of the true and the predicted values of the positive feature model (f_i^+) and the negative feature model (f_i^-) for the three different features used in the model calculation and prediction.

The correlation of the coefficients of the brain actors and the fluid intelligence values are calculated for each subject and averaged over all subjects. The correlation is plotted for the highest positive and negative values in a weighted manner in Figure 5.24 to visualize the brain areas associated with cognitive function.

5.7 Summary

The dataset used for the research of this work is part of the HCP S1200 release [59]. There are 453 subjects in *SubjectGroupA* with four scans per subject. To examine the subject stability the dataset is split into *MainDatasetA* and *ReproductionDatasetA*1 each containing two scans for each of the 453 subjects. NMF is performed on this dataset to create an atlas of $n_c = 60$ brain regions. The reproducibility of the result is measured by calculating the correlation of matching actors. The mean correlation is 0.789 with a standard deviation of 0.268. The value of $n_c = 60$ is chosen because the reproducibility is maximal compared to other values of $n_c > 20$.

The global results W and H are used as an initialisation of a second NMF to create the individual specific results W_i and H_i. In contrast to the global calculation the algorithm has to be stopped to avoid over-fitting. The tolerance of $tol = 10^{-2}$ is chosen as the optimal stopping criterion. The reproducibility of the individualized results is analysed by calculating the within- and across-subject correlation of 1000 randomly chosen subject couples. The within-subject correlation (mean value of 0.887) is significantly higher ($p < 0.001$) than the across-subject correlation (mean value of 0.742).

The coefficient of individuality $\mathbf{r}_i$ is calculated for each subject and its stability is analysed by calculating the correlation (mean correlation of 0.894). The individuality across the

cortex is averaged over the 7 Yeo networks of [17]. The network demonstrating the highest individuality is Visual Attention (mean value of 1.250) and the lowest individuality is observed in the Limbic network (mean value of 1.186).

The coefficient of dynamicity $\mathbf{c}_i^{dyn}$ is calculated for each subject by comparing the actor co-activation and averaged over the 7 Yeo networks of [17]. The Visual and Limbic networks display the highest dynamicity (mean value of 0.573 and 0.568) while the Default network exhibits the lowest dynamicity (mean value of 0.459).

The actor composition at each point on the cortex of an individual subject is used to train a linear model capable of predicting task activation. The quality of the prediction is analysed by calculating the correlation matrix between the predicted and true task activations. There is a significant difference ($p < 0.001$) between the values of the diagonal (mean $\bar{m}_{ii}$) and the off-diagonal (mean $\bar{m}_{i\neq j}$) for six of the seven tasks tested (all but Gambling). The highest quality is obtained for Language 3 ($\bar{m}_{ii} = 0.666$) and the lowest quality for Gambling 2 ($\bar{m}_{ii} = 0.147$).

A linear model is trained to predict cognitive data by using fluid intelligence values f_i as targets. Three different features are used for the model training: the coefficient of individuality, the across-subject correlation and the coefficient of dynamicity. The quality of the prediction is assessed by calculating the correlation of the true and predicted values. The feature resulting in the highest correlation is the coefficient of individuality with a correlation of 0.320 for the negative feature model.

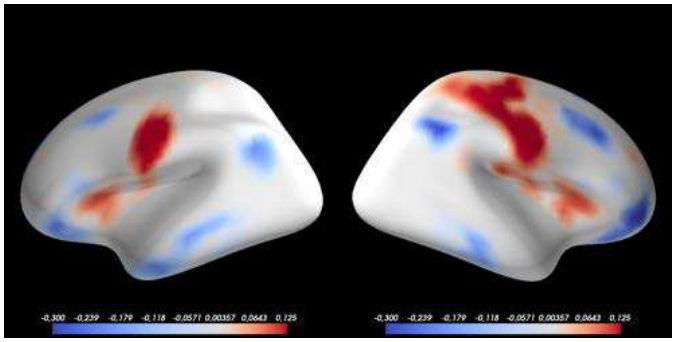

(a) coefficient of individuality

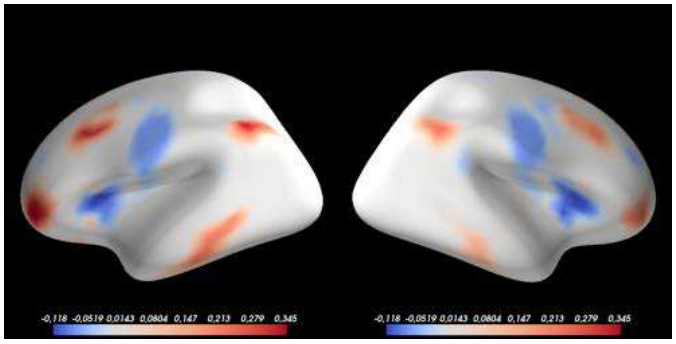

(b) across-subject correlation

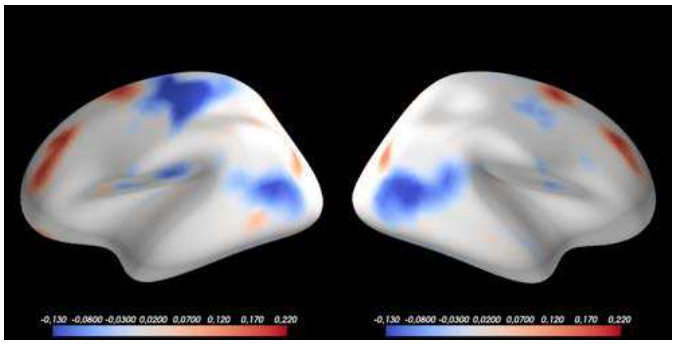

(c) coefficient of dynamicity

Figure 5.24: Correlation between coefficients and fluid intelligence. The correlation is averaged over all subjects and weighted by the global actor footprints on the cortex. The correlation of the highest positive and negative values for the coefficient of individuality (a), the across-subject correlation (b) and the coefficient of individuality (c) are plotted. The images show a lateral view of the left hemisphere (left) and the right hemisphere (right).

CHAPTER 6

Discussion

The results of this work are discussed in this chapter. The main focus lies on the comparison to the state of the art and the interpretation of the implications of the results. The process and results of brain parcellation are discussed in the Section 6.1. Section 6.2 examines the results concerning individuality and Section 6.3 those concerning dynamicity. The task prediction is reviewed in Section 6.4 and the fluid intelligence prediction is debated in Section 6.5. The possibilities for future work are discussed in Section 6.6.

6.1 NMF Results

To create a functional parcellation of the human cerebral cortex brain fMRI data is analysed using NMF. The application of NMF in this context yields two results: the matrix W containing information about the functionally connected brain actors and the matrix H that holds information about activation and co-activation of these actors over the course of time. Because of the non-negativity of the results, they can be directly interpreted. The actors in W are greater than 0 on all points on the cortex of the corresponding actor footprint and equal to 0 everywhere else. One functional region is therefore defined by the points on the cortex where the actor has values greater than 0. This enhances the interpretibility compared to methods that result in positive and negative values (e.g. PCA). The activation of the actors in H behaves in a similar matter. If the actor is active at a given point in time the value is greater than 0 and it is equal to 0 if the actor is not active. The time points of activation can be identified as the time points at which the entry of the corresponding actor is greater 0.

The parcellation calculated in this work demonstrates high reproducibility, analysed by the actor correlation, on a global level ($cor = 0.789$ for $n_c = 60$) as well as on an individual level (average of $cor = 0.887$ for $n_c = 60$).

As stated in [17] it is difficult to evaluate the quality of the parcellation in terms of anatomical and functional interpretibility. For this reason results are calculated for $n_c = 7$ (see (a) in Figure 5.3). The results for $n_c = 7$ show a high similarity to the established results of [17], especially in the default mode network (pink), the frontoparietal network (orange) and even including a similar separation of the sensory and motor cortices (blue and purple) described in [17]. This result proves that NMF is a useful tool to produce an interpretable and reproducible parcellation of the brain.

The result for $n_c = 60$ has the same network structures but the bigger regions are split into subregions, most notable in the sensory and motor cortices mentioned above. While these regions still uphold features of the major networks, the results of $n_c = 120$ show little to none. Most of the regions are evenly distributed and evenly shaped, having lost all interpretibility.

To get an individual-specific parcellation, the global results are used as an initialisation of a second NMF. Using a population based atlas as a starting point for the calculation of an individualized result is a method that has already been applied successfully [6]. Naturally the algorithm has to be stopped at convergence. Therefore the choice of the stopping criterion has a major influence on the quality of the result.

As can be seen in Figure 5.4 the quality of the result drops significantly for $tol < 10^{-2}$ as a stopping criterion. In this case the correlation of actors is used as a measure of quality. The within-subject correlation drops which implies a reduced reproducibility and stability of the method. The decline in the across-subject correlation indicates a lower grade of group-level similarity. The reason for this occurrence is visible in Figure 5.5. The individual actors start to scatter and diverge from the global result, which has two indications: 1. the actors lose their interpretibility and 2. the actors lose their distinctive characteristics. The scattering of the actors acts like an addition of noise, reducing the quality of the result. Though the ratio r which corresponds to the individuality of the result has a lower value for $tol = 10^{-2}$ ($r = 1.2$) compared to values of $tol < 10^{-2}$ ($r = 1.5$ for $tol = 10^{-3}$), the value is high enough to be acceptable as the aforementioned downsides outweigh the drop in individuality and the rise of r. Consequently the values of $tol < 10^{-2}$ are bad choices for the stopping criterion. The black line in Figure 5.4 is the difference $dif = within - across$. It is important for values of $tol > 10^{-2}$ to visualize the change of the global actors. For low numbers of iterations (corresponding to high values for tol) the actors are similar to the global actors and therefore highly similar to each other ($within \approx across \geq 0.9$) with $dif < 0.1$. Hence they are not individual-specific and therefore the values for $tol > 10^{-2}$ are a bad choice as well. In conclusion the optimal stopping criterion is $tol = 10^{-2}$ as the difference dif is significant (i.e. $dif > 0.1$), the within-subject correlation is high ($within > 0.8$) and the ratio r is acceptable.

The final individualized results are consistent among the same subject, evaluated by the high within-subject correlation. It has to be noted however that the individual actors are dependant of the initialisation. As long as the same global initialisation is used for calculations there is no direct problem with this. When the results of two different initialisations are compared one can see that the actors are generated differently. This is

visible in Figure 5.6. Especially in the third row the actor footprint shows two regions in the frontal cortex for $MainDatasetA$ (A) and a single one for $ReproductionDatasetA1$ (A1). This reduces the reproducibility of the algorithm and complicates the interpretation because the same brain region is grouped into different actors. There are two possible solutions for this problem: 1. using fewer regions, then associated regions are not split into multiple actors, or 2. applying an additional clustering algorithm to join regions. These methods are definitely a topic for future research.

There is one initial parameter for the algorithm of NMF: the number of components n_c. It is mentioned in Section 4.3 that the *right* value has to be picked. But what exactly is the *right* value? Finding a definitive answer to that question is challenging and maybe there is no *"single correct answer given that the cerebral cortex possesses complex patterns of diverging and converging connections among areas."* [17]. It is necessary to approach it by limiting the possible candidates. The dataset used has 5124 points of measurement on the cortex. Since the focus of this work lies on the connectivity between these points and the research of functional brain areas, it is necessary to reduce the number of regions so that multiple points are included in each region. For this reason it is desired that a region contains at least 1% of the data points which leads to $n_c = 100$ respectively. In theory, a computation of all possible values can be done to get results for each value of n_c; in practice however this would take a long time and lots of memory. Hence the computation is done in discrete steps for n_c. By comparing the resulting correlations of $n_c = 50$, $n_c = 100$ and $n_c = 150$, a trend is visible. The higher the number of regions the lower the reproducibility of the parcellation. For this work a value of $n_c = 60$ has been chosen because the respective results have the highest reproducibility for values of $20 < n_c < 150$. The numbers of $n_c \leq 20$ indicate better reproducibility, but for the context of this work this number of regions which is low in comparison has no other benefits; whereas more regions equal a finer grained parcellation which is beneficial for this work. In fact a higher number of initial regions can potentially be used to apply additional merging and clustering methods, e.g. as described in [9], for future studies.

6.2 Individuality

The individualized results are analysed in regard to their reproducibility within the same subject and variation across different subjects. For this purpose the correlation of the actor footprints is calculated. The average within-subject correlation is $cor = 0.887$ for the $MainDatasetA$ and $cor = 0.885$ for the $ReproductionDatasetA1$. These values demonstrate high reproducibility within the same subject and indicate high stability of the method. The average across-subject correlation is $cor = 0.742$ for the $MainDatasetA$ and $cor = 0.749$ for the $ReproductionDatasetA1$. This can be interpreted as a high correlation across subjects and hence a stable parcellation that has similar regions independent of the subject. On the other hand these values are significantly lower ($p < 0.001$, see Table 5.3) than the values of the within-subject correlation, indicating a higher variation across different subjects than within the same subject. This is an important finding illustrating that the individual-specific differences vary across subjects

but are reproducible within the same subject. The variation of these individual-specific differences is analysed by calculating the coefficient of individuality r_i defined by (4.10).

To evaluate the quality of this result it is necessary to compare it to previous work. As stated in Section 2.3.1 Wang et al. [6] have researched the individualization as well as the within-subject reproducibility and across-subject variability in this context. It is important to note that their results are calculated using the Dice coefficient (opposed to the correlation used in this work). However both values indicate the same results and can be compared for the interpretation of the individualization quality. Wang et al. [6] have calculated 0.83 and 0.824 for the within-subject reproducibility. The results of this work (0.887 and 0.885) are similar but higher indicating a higher stability of the method within the same subject. The across-subject values of [6] (0.67 and 0.605) however are different (especially 0.605), as the results of this work are higher (0.742 and 0.749). There are two possible explanations for this: 1. The results of this work are closer to the global initialisation and therefore more similar across subjects; and 2. the disparity is caused by the different calculations, as the dice coefficient is more sensible to differences that may be less relevant (e.g. at the borders of regions). As mentioned above one has to be careful when comparing two differently calculated coefficients (in this case the Dice coefficient and the correlation) but the resulting indication is the same: The within-subject reproducibility is significantly different from the across-subject variability and the within-subject values are significantly higher than the across-subject values.

The differences in individuality across the cortex (see Figure 5.10) have been analysed in previous works as mentioned in Section 2.3. The research of Laumann et al. [27] has concluded high individuality in the medial, fronto-parietal and default mode regions. A similar result is acquired in this work. The values indicative of individuality of r in these regions are high ($r > 1$, colour red in Figure 5.10). The lower values in the somato-motoric regions match the results of [27] with low across-subject variability and low individuality.

Analogous to these results, the findings of Langs et al. [8] and Finn et al. [29] (see Section 2.3.3 and Section 2.3.6) have determined the location of the networks most relevant for individuality in the frontal, temporal and parietal lobes. While these areas demonstrate high individuality, the motoric and visual areas display lower individuality. The results provided in this work directly correspond to this conclusion.

The consistency in the findings of this work and the state of the art validates the quality of the results concerning the individualization. The further research of within- and across-subject differences leads to the calculation of individuality and matches the existing results from previous works.

The low individuality averaged across the Motor, Visual and Limbic Yeo-7 regions of [17] (see Figure 5.11) is a clear implication that the basic physical regulation networks are highly similar for each individual subject. The more complex areas of Attention (VA and DA) as well as the Fronto-Parietal network are more specific for each individual and indicate the influence of hereditary differences and differences in the life of the subjects

(upbringing, education, experiences, interests, etc.). The results of Müller et al. [26] are similar though the descending order is different (e.g. with the lowest value being the Visual network). The overall structure is the same as in this work: the Default network in the center with the Attention and Fronto-Parietal networks above and the Motor, Visual and Limbic networks below. One noteworthy disparity is the high difference between the Limbic and the Motor and Visual networks whereas the result for the Motor region in this work is close to the value of the Default network. A possible cause for this disparity is the dataset used. 23 subjects are used in [26] (with 5 scans per subject) whereas 453 subjects are used in this work (with 2 scans per subject). The different dataset may explain the difference in the descending sequence while maintaining the same overall indications.

The results of this work demonstrate differences in individuality across the cortex yet the values are highly similar to each other (all between 1.15 and 1.25). This is explained by the calculation of the coefficient of individuality r. A better calculation has yet to be found and may be a topic for further research.

The individual differences are relevant for clinical applications [8] [26]. The individuality is likely to be connected to the susceptibility of neuropsychiatric disorders [26]. Studies have found that the cause might be a disconnection of regions in functional networks. This finding is supported by the time period many neuropsychiatric diseases emerge: adolescence [26]. During this period the long-range connections in the brain are formed and abnormal or absent connections may result in a higher susceptibility for mental diseases [26]. Especially abnormal activity at rest and disconnections in the default network are identified to be indicators for diseases like attention deficit hyperactivity disorder [61] or depression [62] as well as Alzheimer's disease [63] [64]. The research of brain networks and their individual differences could allow an early detection of the increased susceptibility and facilitate an improved treatment or even the prevention of neuropsychiatric diseases.

The knowledge of the individuality of brain regions is important for pre-operative planning [26]. If the individuality of the region containing the operation site is high, additional imaging and examination are required. The same is true for brain stimulation therapy: depending on the individuality of the target area, it might be necessary to obtain additional information of the specific subject's connectivity pattern instead of using group averaged data [26].

6.3 Dynamicity

The differences in dynamicity across the cortex demonstrate a similar picture: the values for the primary motor cortex and the primary somatosensory cortex are significantly lower than the rest of the cortex. This can be seen in Figure 5.13 (dark blue region) and could be explained by the complexity of the corresponding function of the region as well as its evolutionary expansion. In contrast to the frontal, temporal and parietal lobes who are *"phylogenetically late-developing regions"* [26] the motor region is a primal region and

has therefore little connection to the areas that developed later. This is also beneficial from an evolutionary point of view as the movement responses have to be quick and the involvement of different regions potentially increases the reaction time.

Averaging the coefficients of dynamicity for each area of the Yeo-7 atlas [17] (see Figure 5.14) yields a result that has to be discussed. First of all the low values in the motor region mentioned above are equalized by the high values in the upper half of the temporal lobe (that is still part of the Motor network of [17]). The lower half of the temporal lobe has low values of dynamicity (yellow-teal in Figure 5.13) and the corresponding Default network is therefore the network with the lowest dynamicity. The Default network is deactivated during most tasks [1] which implies low co-activation with other brain networks. The actors in the Default network therefore mainly show co-activation with other actors of the same network when they are active resulting in a low value of dynamicity. The network demonstrating the highest dynamicity is the Visual network. The reason for this lies in the function of this network: the processing of visual inputs. The information gained from this processed data is transferred to specialized regions all over the cortex [1]. This means the Visual network displays co-activation with many other brain regions which results in a high value of dynamicity. The Limbic network also exhibits high dynamicity. The area corresponding to this network encircles the brain stem and is connected to the experience and expression of emotion [1]. Because there is a diversity of emotions each associated with different brain regions this network has a high coefficient of dynamicity.

A comparison of Figure 5.14 and Figure 5.11 implies an inverse relation: the networks with the highest dynamicity (Vis, Lim, and Mot) have the lowest individuality whereas networks with high individuality (FP, VA, DA) have lower values of dynamicity.

6.4 Task Prediction

The data acquisition of the fMRI occurs in different settings. The data used in this work is resting-state data which means the subjects do not perform any task. It is possible to obtain fMRI data while the subjects perform different tasks as well. There is a connection between the actor activation at rest and during tasks [14]. This means the task activation can be predicted using task-free data. In this work the individual actor composition at a point on the cortex is used as the feature of a linear model to predict the task activation at this point on the cortex. All points on the cortex of all but one subjects are used to train the model and test it in a leave-one-out fashion.

The model is capable of predicting the task activation using task-free data. The two-tailed t-test statistics show that the predicted activation is more similar to the actual activation of the corresponding subject than to the actual activation of all the other subjects. The only exception is the task Gambling 2. For this task the difference is only significant for $p > 0.043$. As can be seen in Figure 5.19, the overlap of the diagonal and off-diagonal entries includes the entire distribution. In Figure 5.20 one can see that part of the distribution of the normalized values is greater than 1 which indicates a low prediction

quality because the correlation between the predicted and actual activation is higher for non-corresponding couples. The main reason for this lies in the method used. The brain data used in this work and all subsequent results are 2D surface data of the cortex. Therefore 3D effects like the activation of subcortical gray matter are excluded. For tasks that are connected or based on these effects the model training fails and therefore the prediction quality is comparatively bad. Gambling is a task that is restricted to subcortical gray matter [28]. To improve the prediction quality for this task it is necessary to include additional features representing the subcortical activation in the training of the model.

The tasks Emotion, Language, Motor, Relational, Social and WM all display a minimal number of values greater than 1 in Figure 5.20. This demonstrates the prediction quality for these tasks as there is a significant difference between the diagonal and off-diagonal values and more than 90% of the distribution of the off-diagonal values is smaller than 1.

The best predictions are given for the tasks Language ($\bar{m}_{ii} = 0.666, t = 23.6$) and WM ($\bar{m}_{ii} = 0.660, t = 10.6$), followed closely by Motor ($\bar{m}_{ii} = 0.608, t = 10.1$) and Emotion ($\bar{m}_{ii} = 0.608, t = 7.3$). In Figure 5.19 the distributions of the diagonal and off-diagonal correlation values display less overlap (than Gambling) and the difference in the means is visible. The results for the tasks Social ($\bar{m}_{ii} = 0.437, t = 8.9$) and Relational ($\bar{m}_{ii} = 0.332, t = 3.8$) in comparison are worse. To find the cause of this difference in quality it is necessary to look at the task activation on the cortex in Figure 5.21. The images in (b) show the actual and predicted task activation for the Language task. In both pictures the activation is mainly restricted to the language area in the temporal lobe with smaller areas of activation in the frontal and parietal lobes. The activation for the WM task is also mainly restricted to a specific brain region in the occipital lobe. In contrast to these tasks, the activation for the Gambling and Relational tasks are not restricted to a specific brain region. As can be seen in (a) and (c) the task activation is scattered across the cortex. This could be explained by the complexity of the tasks: many brain regions participate and cooperate during these tasks. In addition subcortical gray matter activation is included as well. The simple model used in this work is not capable of learning all these dependencies. This is reflected in the absolute values of the predicted task activations: the true activation values are in the range of 10^0 (Gambling $[-2.85, 2.24]$ and Relational $[-5.47, 2.83]$) while the values of the prediction are in the range of 10^{-1} (Gambling $[-0.154, -0.0534]$ and Relational $[-0.156, 0.102]$).

To evaluate the quality of the results they are compared to the state of the art results of [28]. For this reason the same tasks have been chosen for the prediction. The resulting $\bar{m}_{ii}$ of the tasks Language 3 (0.72) and WM 9 (0.74) are similar but slightly higher than the results of this work (0.67 and 0.66). The outcome of the tasks Emotion 3 (0.57) and Motor 7 (0.56) are comparable but marginally better in this work (0.61 and 0.61). For these four tasks the results display high similarity therefore confirming the functionality of the model. The remaining three tasks are the ones with the lowest quality results. It is interesting that there is no significant drop in quality for these tasks in [28]. On the contrary: the values for Gambling 2 (0.74), Relational 2 (0.80) and Social 2 (0.76)

are as high or even higher than the aforementioned ones, unlike the results of this work (0.15, 0.33, and 0.44). The reason for this discrepancy is the different feature set used for the prediction model. The model of [28] uses functional connectivity at rest as well as *"predictors encoding individual brain morphology (gross structure) and microstructure"* [28]. In total the number of features used in [28] is 107 while in this work it is $n_c = 60$. The additional features enhance the quality of the prediction of tasks that display less restriction to specific brain regions (i.e. Gambling and Relational). Regardless it is mentioned in [28] that the quality for Gambling 2 is lower with the explanation given above (subcortical gray matter restriction).

The results of this work indicate that it is possible to predict the activation of specific tasks using task-free data acquired at rest. This enables the task prediction of subjects who are unable to perform the task (e.g. because of medical conditions). To enhance the prediction quality however it is necessary to improve the model by including additional features especially regarding the activations in the subcortical gray matter.

6.5 Fluid Intelligence Prediction

The individuality and dynamicity of the brain regions of an individual subject are correlated to the fluid intelligence of the same subject. The comparison of the true and predicted values of fluid intelligence display that there is a significant correlation (0.320) when using the coefficient of individuality as a feature. It has to be noted that this is only true for the negative feature model f_i^-. The reason for this is the inverse dependence of the across-subject correlation as the coefficient of individuality is defined as $r = \frac{within}{across}$. The across-subject correlation is researched as a predictive feature for the model as well and demonstrates a significant correlation for the positive feature model f_i^+ (0.301). In comparison the quality of the prediction using the coefficient of dynamicity is lower (0.218). For all three features the model fails to predict the whole range of fluid intelligence. As can be seen in Figure 5.22 the predicted values are mostly in the range $[10, 20]$ resulting in big errors for values $f_i < 10$ or $f_i > 20$. The results are scattered around the mean value and are generally lower for values $f_i < 15$ and higher for values $f_i > 15$. Hence the model is able to successfully predict the fluid intelligence and give an estimate of the height of the value in regard to the mean.

The actors that are chosen for the predictive model training are visualized in Figure 5.24. The images corresponding to the coefficient of individuality (Figure 5.24 (a)) and the across-subject correlation (Figure 5.24 (b)) display similar patterns but with an opposite sign. This is explained by the calculation of the coefficient of individuality because it is inversely dependent on the across-subject correlation. The features yielding the best prediction results (negative for the coefficient of individuality and positive for the across-subject correlation) are four regions scattered across the cortex (blue in Figure 5.24 (a) and red in Figure 5.24 (b)). The pattern is reminiscent of the patterns of the Default and especially the Fronto-Parietal networks which means that these two networks could be closely correlated to fluid intelligence. While the results for the coefficient of

dynamicity are part of the Fronto-Parietal and Default networks as well, they display no similarity to the other results, which interferes with this hypothesis. The features yielding the best results are positive and concentrated in regions of the frontal lobe and small regions in the occipital lobe.

To assess the quality of these results it is necessary to compare them to existing research. The experiment has been designed with this purpose in mind and uses the same number of subjects and the same model calculation as the work of Finn et al. [29]. The resulting correlation of true and predicted fluid intelligence is 0.5 in [29]. This value is higher than the values of this work. The reason for this is the difference in features for the predictive model as the researchers of [29] use the connectivity profiles. By looking at the graph comparing predicted and true values one can see that the values are distributed in a similar fashion as in Figure 5.23. Analogous to this work the predicted values are mostly in the range $10 \leq f_i \leq 20$ and scattered around the mean. The prediction quality for values $f_i > 15$ however is better compared to the results of this work therefore resulting in a higher total correlation.

6.6 Future Work

The application of NMF for the analysis of human brain fMRI data has significant benefits over other parcellation techniques like PCA. The main advantages are the interpretibility of the results and the dimensionality reduction of the data. However there are three major areas that can still be improved and have to be further investigated in future work: 1. the parcellation, 2. the coefficient calculation, 3. the prediction.

1. The parcellation: The NMF algorithm requires one significant input parameter: the number of components n_c. For the calculations of this work a value of $n_c = 60$ is chosen because of the high reproducibility (actor correlation of 0.789) however values of $n_c < 40$ demonstrate higher stability (actor correlation of 0.891 for $n_c = 20$ and 0.971 for $n_c = 7$). For the purpose of this work a higher number of components is beneficial but that may not be the case for future research. The number of regions could also be reduced by applying a clustering algorithm to fuse functionally connected regions. This process could be formulated in a dynamic manner resulting in different numbers of regions dependent on the individual subject. This way abnormalities in the brain function could be revealed and physical or mental illnesses could be detected.

2. The coeeficient calculation: In this work the concepts of the coefficient of individuality and the coefficient of dynamicity are introduced. The coefficient of individuality is calculated by comparing the within- and across-subject correlation of the brain actors. This way the individuality is calculated by comparing the individual regions to those of all the other subjects in the dataset. While this method is functional it can still be improved. It could be beneficial to calculate the coefficient by comparing the individual actors to a global average. For the comparison the correlation is calculated resulting in a scalar for each actor. A more complex calculation could provide information answering additional questions e.g. *What part of the region indicates higher individuality?* or *Is the*

individuality continuously spread across the region? This may be obsolete for sufficiently small regions but could be relevant for larger regions (i.e. a lower number of components). The coefficient of dynamicity is calculated by comparing the actor co-activation over time. This is a novel concept introduced in this work and is therefore difficult to review. For the calculation only the top 10% i.e. 6 actors are included - the inclusion of more or all actors might improve the results especially if the number of included actors is chosen in a dynamic manner. This way the calculation would be different for actors with few (e.g. 2) and many (e.g. 15) co-actors. A different definition and calculation could also improve the quality of the results.

3. The prediction: First of all the prediction model could be changed and improved. In this work linear models are used. While more complex models or machine learning algorithms (e.g. neural networks) could improve the prediction quality they usually require more computational power and training data. The task activation can be predicted with the (task-free) matrix W_i. An improvement of the predictive model would be the inclusion of temporal data. The task activation could be predicted in a dynamic matter instead of a static snapshot by including H_i as a model feature. This would allow the simulation of the brain activity during tasks potentially in real time enabling the research of the dynamic connections of brain areas and emulating them for subjects who cannot perform certain tasks (e.g. due to illness). The inclusion of additional features (e.g. microstructural or subcortical) could also enhance the prediction quality.
The prediction of fluid intelligence is performed with a linear model and different coefficients as features. For all coefficients used the quality of the prediction is decent but lower compared to the state of the art results. To provide a more accurate estimation of the fluid intelligence for an individual subject the model has to be improved. This can be achieved by filtering the training data to exclude outliers or by using a more complex model. The inclusion of additional or different features in the model training may also improve the prediction quality. An increase of the amount of training data could enhance the prediction quality as well.

CHAPTER 7

Conclusion

The results of this thesis have demonstrated that NMF can be used to analyse brain fMRI data and create of an atlas of brain regions that is reproducible and anatomically interpretable. It is possible to create individual-specific results that display high reproducibility within the same subject while exhibiting significant variation across different subjects. The individuality of brain regions can be quantified and is distributed unevenly across the cortex with high values in the network of Dorsal-Attention and low values in the Limbic network. The brain actor dynamics and co-activations are quantified by the coefficient of dynamicity. There is a variation in dynamicity across the cortex and the regions displaying the highest dynamicity are in the Visual and Limbic networks while the Default network exhibits the lowest dynamicity.

Individual task activation can be predicted using task-free individualized data, i.e. the brain actor composition, as training. The prediction quality is high for all but one task (Gambling) but additional features e.g. of the subcortical gray matter could conceivably increase the performance. It is possible to predict cognitive data like fluid intelligence using the coefficient of individuality and the coefficient of dynamicity. However the predictive model is limited and the quality of the prediction can still be improved.

In conclusion NMF is a useful tool for brain fMRI analysis and the individual subject specific results obtained could be relevant for clinical application. The knowledge of individuality and dynamicity could be important for pre-operative planning and brain stimulation therapy as well as the estimation of susceptibility for neuropsychiatric disorders and possibly an improved or even preventative treatment of mental diseases. The prediction of task activation could be used for patients who are unable to perform certain tasks. For the actual use in clinical practice however it is necessary to continue the research and further improve the quality and reproducibility of the results.

Bibliography

[1] Mark Bear, Barry Connors, and Michael Paradiso. *Neuroscience: Exploring the brain: Fourth edition*. Wolters Kluwer, 2015.

[2] Christopher Honey, Rolf Kötter, Michael Breakspear, and Olaf Sporns. Network structure of cerebral cortex shapes functional connectivity on multiple time scales. *Proceedings of the National Academy of Sciences of the United States of America*, 104:10240–10245, 2007.

[3] Steven Bressler. Large-scale cortical networks and cognition. *Brain research. Brain research reviews*, 20:288–304, 1995.

[4] Jason Hill, Donna Dierker, Jeffrey Neil, Terrie Inder, Andrew Knutsen, John Harwell, Timothy Coalson, and David Van Essen. A surface-based analysis of hemispheric asymmetries and folding of cerebral cortex in term-born human infants. *The Journal of neuroscience : the official journal of the Society for Neuroscience*, 30:2268-2276, 2010.

[5] Matthew Brett, Ingrid Johnsrude, and Adrian Owen. The problem of functional localization in the human brain. *Nature reviews. Neuroscience*, 3:243-249, 2002.

[6] Danhong Wang, Randy L. Buckner, Michael D. Fox, Daphne J. Holt, Avram J. Holmes, Sophia Stöcklein, Georg Langs, Ruiqi Pan, Tianyi Qian, Kuncheng Li, Justin T. Baker, Steven M. Stufflebeam, Kai Wang, Xiaomin Wang, Bo Hong, and Hesheng Liu. Parcellating cortical functional networks in individuals. *Nat Neurosci*, 18(12):1853–1860, 2015.

[7] Evan Gordon, Timothy Laumann, Babatunde Adeyemo, Adrian Gilmore, Steven Nelson, Nico Dosenbach, and Steve Petersen. Individual-specific features of brain systems identified with resting state functional correlations. *NeuroImage*, 146, 2016.

[8] Georg Langs, Danhong Wang, Polina Golland, Sophia Stöcklein (nee Müller), Ruiqi Pan, Mert Sabuncu, Wei Sun, Qiao Li, and Hesheng Liu. Identifying shared brain networks in individuals by decoupling functional and anatomical variability. *Cerebral Cortex*, 26, 2015.

[9] Thomas Blumensath, Timothy E. J. Behrens, and Stephen M. Smith. Resting-state fmri single subject cortical parcellation based on region growing. *Medical Image Computing and Computer-Assisted Intervention (MICCAI)*, 7511:188–195, 2012.

[10] Kenneth K. Kwong, John W. Belliveau, David A. Chesler, Inna Goldberg, Robert M. Weisskoff, Brigitte P. Poncelet, David Kennedy, Bernice Hoppel, Mark Cohen, and Robert Turner. Dynamic magnetic resonance imaging of human brain activity during primary sensory stimulation. *Proceedings of the National Academy of Sciences of the United States of America*, 89:5675-5679, 1992.

[11] Seiji Ogawa, David W. Tank, Ravi Menon, Jutta M. Ellermann, Seong-Gi Kim, Hellmut Merkle, and Kamil Ugurbil. Intrinsic signal changes accompanying sensory stimulation: functional brain mapping with magnetic resonance imaging. *Proceedings of the National Academy of Sciences of the United States of America*, 89:5951-5955, 1992.

[12] Randy Buckner and Justin Vincent. Unrest at rest: Default activity and spontaneous network correlations. *NeuroImage*, 37:1091–1096; discussion 1097, 2007.

[13] Stephen Smith, Karla Miller, Steen Moeller, Junqian Xu, Edward Auerbach, Mark Woolrich, Christian Beckmann, Mark Jenkinson, Jesper Andersson, Matthew Glasser, David Essen, David Feinberg, Essa Yacoub, and Kamil Ugurbil. Temporally-independent functional modes of spontaneous brain activity. *Proceedings of the National Academy of Sciences of the United States of America*, 109:3131–3136, 2012.

[14] Stephen Smith, Peter Fox, Karla Miller, David Glahn, P. Fox, Clare Mackay, Nicola Filippini, Kate Watkins, Roberto Toro, Angela Laird, and Christian Beckmann. Correspondence of the brain's functional architecture during activation and rest. *Proceedings of the National Academy of Sciences of the United States of America*, 106:13040–13045, 2009.

[15] Hongming Li, Theodore D. Satterthwaite, and Yong Fan. Large-scale sparse functional networks from resting state fmri. *Neuroimage*, 156:1–13, 2017.

[16] Harold W. Kuhn. The hungarian method for the assignment problem. *Naval Research Logistics Quarterly*, 2:83-97, 1955.

[17] B. T. Thomas Yeo, Fenna M. Krienen, Jorge Sepulcre, Mert R. Sabuncu, Danial Lashkari, Marisa Hollinshead, Joshua L. Roffman, Jordan W. Smoller, Lilla Zöllei, Jonathan R. Polimeni, Bruce Fischl, Hesheng Liu, and Randy L. Buckner. The organization of the human cerebral cortex estimated by intrinsic functional connectivity. *J Neurophysiol*, 106(3):1125–1165, 2011.

[18] Guilherme Ribas. The cerebral sulci and gyri. *Neurosurgical focus*, 28, 2010.

[19] Grazyna Rajkowska and Patricia Goldman-Rakic. Cytoarchitectonic definition of prefrontal areas in the normal human cortex: I. remapping of areas 9 and 46 using quantitative criteria. *Cerebral cortex (New York, N.Y. : 1991)*, 5:307-322, 1995.

[20] Korbinian Brodmann. Vergleichende lokalisationslehre der großhirnrinde. *J. Nerv. Ment. Dis.*, 37:783-784, 1909.

[21] Constantin von Economo and Georg N. Koskinas. *Die Cytoarchitektonik der Hirnrinde des erwachsenen Menschen*. Springer Berlin, 1925.

[22] Lazaros Triarhou. *The Cytoarchitectonic Map of Constantin von Economo and Georg N. Koskinas*, pages 33–53. Springer Berlin, 2013.

[23] Oskar Vogt. Die myeloarchitektonische felderung des menschlichen stirnhirns. *J. Psychol. Neurol.*, 15:221–238, 1910.

[24] Milos Judas and Maja Cepanec. Oskar vogt: The first myeloarchitectonic map of the human frontal cortex. *Translational Neuroscience*, 1:72-94, 2010.

[25] Simon Eickhoff, Nathan Walters, Axel Schleicher, Jillian Kril, Gary Egan, Karl Zilles, John Watson, and Katrin Amunts. High-resolution mri reflects myeloarchitecture and cytoarchitecture of human cerebral cortex. *Human brain mapping*, 24:206-215, 2005.

[26] Sophia Müller, Danhong Wang, Michael D. Fox, B. T. Thomas Yeo, Jorge Sepulcre, Mert R. Sabuncu, Rebecca Shafee, Jie Lu, and Hesheng Liu. Individual variability in functional connectivity architecture of the human brain. *Neuron*, 77(3):586–595, 2013.

[27] Timothy O. Laumann, Evan M. Gordon, Babatunde Adeyemo, Abraham Z. Snyder, Sung Jun Joo, Mei-Yen Chen, Adrian W. Gilmore, Kathleen B. McDermott, Steven M. Nelson, Nico U. F. Dosenbach, Bradley L. Schlaggar, Jeanette A. Mumford, Russell A. Poldrack, and Steven E. Petersen. Functional system and areal organization of a highly sampled individual human brain. *Neuron*, 87(3):657–670, 2015.

[28] Ido Tavor, O. Parker Jones, Rogier B. Mars, S. M. Smith, Timothy E. J. Behrens, and Saad Jbabdi. Task-free mri predicts individual differences in brain activity during task performance. *Science*, 352(6282):216–220, 2016.

[29] Emily S. Finn, Xilin Shen, Dustin Scheinost, Monica D. Rosenberg, Jessica Huang, Marvin M. Chun, Xenophon Papademetris, and R. Todd Constable. Functional connectome fingerprinting: Identifying individuals using patterns of brain connectivity. *Nat Neurosci*, 18(11):1664–1671, 2015.

[30] Ian Jolliffe. Principal component analysis. *Lovric M. (eds) International Encyclopedia of Statistical Science.*, Springer, Berlin, Heidelberg, 2011.

[31] Lars Hansen, Jan Larsen, Finn Nielsen, Stephen Strother, Egill Rostrup, Rober Savoy, Nicholas Lange, John Sidtis, Claus Svarer, and Olaf Paulson. Generalizable patterns in neuroimaging: How many principal components? *NeuroImage*, 9:534-544, 1999.

[32] Stephen Strother, Jon Anderson, Kirt Schaper, John Sidtis, Jyue Liow, Roger Woods, and David Rottenberg. Principal component analysis and the scaled subprofile model compared to intersubject averaging and statistical parametric mapping: I. "functional connectivity" of the human motor system studied with [15o]water pet. *Journal of cerebral blood flow and metabolism : official journal of the International Society of Cerebral Blood Flow and Metabolism*, 15:738-753, 1995.

[33] Karl Friston, Chris Frith, Peter Liddle, and Richard Frackowiak. Functional connectivity: The principal-component analysis of large (pet) data sets. *Journal of cerebral blood flow and metabolism : official journal of the International Society of Cerebral Blood Flow and Metabolism*, 13:5-14, 1993.

[34] Odelia Schwartz, E. J. Chichilnisky, and Eero Simoncelli. Characterizing neural gain control using spike-triggered covariance. In *Advances in Neural Information Processing Systems 14*, volume 14:269-276. MIT Press, 2001.

[35] Hugo Hiden, Georgios Pitsilis, and Watson Paul. Principal components analysis of spike train data: Towards an architecture for the carmen project. In *Proceedings of the UK E-Science All Hands Meeting*. National e-Science Centre, 2007.

[36] Takashi Takekawa, Yoshikazu Isomura, and Tomoki Fukai. Spike sorting of heterogeneous neuron types by multimodality-weighted pca and explicit robust variational bayes. *Frontiers in neuroinformatics*, 6:5, 2012.

[37] Lawrence Sirovich and M. Kirby. Low-dimensional procedure for the characterization of human faces. *Journal of the Optical Society of America. A, Optics and image science*, 4:519-524, 1987.

[38] Matthew A. Turk and Alex P. Pentland. Face recognition using eigenfaces. In *Proceedings. 1991 IEEE Computer Society Conference on Computer Vision and Pattern Recognition*, pages 586–591, 1991.

[39] Hyeonjoon Moon and P. Jonathon Phillips. Computational and performance aspects of pca-based face-recognition algorithms. *Perception*, 30:303–321, 2001.

[40] Aristeidis Sotiras, Susan M. Resnick, and Christos Davatzikos. Finding imaging patterns of structural covariance via nonnegative matrix factorization. *Neuroimage*, 108:1–16, 2015.

[41] Aapo Hyvärinen and Erkki Oja. Independent component analysis: Algorithms and applications. *Neural Networks*, 13(4-5):411-430, 2000.

[42] Christian Beckmann, Marilena DeLuca, Joseph Devlin, and Stephen Smith. Investigations into resting-state connectivity using independent component analysis. *Philosophical transactions of the Royal Society of London. Series B, Biological sciences*, 360:1001–1013, 2005.

[43] Ricardo N. Vigário. Extraction of ocular artefacts from eeg using independent component analysis. *Electroencephalography and Clinical Neurophysiology*, 103(3):395-404, 1997.

[44] Yandong Li, Zhongwei Ma, Wenkai lu, and Yanda Li. Automatic removal of the eye blink artifact from eeg using an ica-based template matching approach. *Physiological measurement*, 27:425–436, 2006.

[45] Debiprasad Acharya and Gitishree Panda. A review of independent component analysis techniques and their applications. *IETE Technical Review*, 25, 2008.

[46] Andrzej Cichocki and Shun-ichi Amari. *Adaptive Blind Signal and Image Processing: Learning Algorithms and Applications*. John Wiley & Sons, 2002.

[47] Ali Al-Saegh. Independent component analysis for separation of speech mixtures: A comparison among thirty algorithms. *Iraqi Journal for Electrical And Electronic Engineering*, 11, 2015.

[48] Zaid Omar, Tania Stathaki, Musa Mokji, and Lila Izhar. A hybrid chebyshev-ica image fusion method based on regional saliency. *Telkomnika (Telecommunication Computing Electronics and Control)*, 15:934-941, 2017.

[49] Daniel D. Lee and H. Sebastian Seung. Algorithms for non-negative matrix factorization. *Advances in Neural Information Processing*, 13 (Proc. NIPS*2000), 2001.

[50] Jae Sung Lee, D. D. Lee, Seungjin Choi, Kwang Suk Park, and Dong Soo Lee. Non-negative matrix factorization of dynamic images in nuclear medicine. In *2001 IEEE Nuclear Science Symposium Conference Record (Cat. No.01CH37310)*, volume 4:2027-2030, 2001.

[51] Tatsuya Yokota, Kazuya Kawai, Muneyuki Sakata, Yuichi Kimura, and Hidekata Hontani. Dynamic pet image reconstruction using nonnegative matrix factorization incorporated with deep image prior. In *2019 IEEE/CVF International Conference on Computer Vision (ICCV)*, pages 3126–3135, 2019.

[52] Olivier Berné, Alexander Tielens, Paolo Pilleri, and Christine Joblin. Non-negative matrix factorization pansharpening of hyperspectral data: An application to mid-infrared astronomy. In *2010 2nd Workshop on Hyperspectral Image and Signal Processing: Evolution in Remote Sensing*, pages 1–4, 2010.

[53] Ibrahim Selim, Eng Arabi, and Bassant M. El. Galaxy image classification using non-negative matrix factorization. *International Journal of Computer Applications*, 137:4-8, 2016.

[54] David Guillamet and Jordi Vitrià. Non-negative matrix factorization for face recognition. In *Topics in Artificial Intelligence*, pages 336–344. Springer Berlin Heidelberg, 2002.

[55] Yang Zhao, Huiyang Wang, and Jihong Pei. Deep non-negative matrix factorization architecture based on underlying basis images learning. *IEEE Transactions on Pattern Analysis and Machine Intelligence*, PP, 2019.

[56] Fabian Pedregosa, Gaël Varoquaux, Alexandre Gramfort, Vincent Michel, Bertrand Thirion, Olivier Grisel, Mathieu Blondel, Peter Prettenhofer, Ron Weiss, Vincent Dubourg, Jake Vanderplas, Alexandre Passos, David Cournapeau, Matthieu Brucher, Matthieu Perrot, and Édouard Duchesnay. Scikit-learn: Machine learning in Python. *Journal of Machine Learning Research*, 12:2825-2830, 2011.

[57] Michael Fox and Marus Raichle. Spontaneous fluctuations in brain activity observed with functional magnetic resonance imaging. *Nature reviews. Neuroscience*, 8:700–711, 2007.

[58] John Raven. The raven's progressive matrices: change and stability over culture and time. *Cognitive psychology*, 41(1):1-48, 2000.

[59] David C. Van Essen, Kamil Ugurbil, Edward Auerbach, Deanna Barch, Timothy E. J. Behrens, Richard Bucholz, A. Chang, Liyong Chen, Maurizio Corbetta, Sandra Curtiss, Stefania Della Penna, David Feinberg, Matthew Glasser, Noam Harel, Andrew C. Heath, Linda Larson-Prior, Daniel Marcus, Georgios Michalareas, Steen Moeller, and Essa Yacoub. The human connectome project: A data acquisition perspective. *NeuroImage*, 62:2222-2231, 2012.

[60] Matthew F. Glasser, Stamatios N. Sotiropoulos, J. Anthony Wilson, Timothy S. Coalson, Bruce Fischl, Jesper L. Andersson, Junqian Xu, Saad Jbabdi, Matthew Webster, Jonathan R. Polimeni, David C. Van Essen, and Mark Jenkinson. The minimal preprocessing pipelines for the human connectome project. *NeuroImage*, 80:105, 2013.

[61] Lixia Tian, Tianzi Jiang, Yufeng Wang, Yu-Feng Zang, Yong He, Meng Liang, Manqiu Sui, Qingjiu Cao, Siyuan Hu, Miao Peng, and Yan Zhuo. Altered resting state functional connectivity patterns of anterior cingulate cortex in adolescents with attention deficit hyperactivity disorder. *Neuroscience letters*, 400:39–43, 2006.

[62] Amit Anand, Yu Li, Yang Wang, Jingwei Wu, Sujuan Gao, Lubna Bukhari, Vincent Mathews, Andrew Kalnin, and Mark Lowe. Activity and connectivity of brain mood regulating circuit in depression: A functional magnetic resonance study. *Biological psychiatry*, 57:1079–1088, 2005.

[63] Michael Greicius, Gaurav Srivastava, and Vinod Menon. Default-mode network activity distinguishes alzheimer's disease from healthy aging: Evidence from functional mri. *Proceedings of the National Academy of Sciences of the United States of America*, 101:4637–4642, 2004.

[64] Liang Wang, Yu-Feng Zang, Yong He, Meng Liang, Xinqing Zhang, Lixia Tian, Tao Wu, Tianzi Jiang, and Qiao Li. Changes in hippocampal connectivity in the

early stages of alzheimer's disease: evidence from resting state fmri. *NeuroImage*, 31:496–504, 2006.